




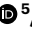


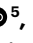





# Investigation of the enhanced antitumour potency of STING agonist after conjugation to polymer nanoparticles

Received: 20 December 2021

Accepted: 31 May 2023

Published online: 13 July 2023

 Check for updates

Pere Dosta <sup>1,2,3</sup>✉, Alexander M. Cryer <sup>1,2,3</sup>, Michelle Z. Dion <sup>1,2,3,4</sup>, Tsubasa Shiraishi <sup>5</sup>, Steven P. Langston <sup>5</sup>, David Lok<sup>5</sup>, Jianing Wang<sup>5</sup>, Sean Harrison<sup>5</sup>, Tiquella Hatten <sup>5</sup>, Michelle L. Ganno <sup>5</sup>, Vicky A. Appleman <sup>5</sup>, Gonzalo Muñoz Taboada <sup>6</sup>, Núria Puigmal <sup>1,2,3</sup>, Shiran Ferber<sup>1,2</sup>, Santhosh Kalash<sup>1,2</sup>, Michaela Prado <sup>1,2</sup>, Alma L. Rodriguez<sup>1,2</sup>, Walid S. Kamoun<sup>5</sup>, Adnan O. Abu-Yousif<sup>5</sup> & Natalie Artzi <sup>1,2,3</sup>✉

Intravenously administered cyclic dinucleotides and other STING agonists are hampered by low cellular uptake and poor circulatory half-life. Here we report the covalent conjugation of cyclic dinucleotides to poly( $\beta$ -amino ester) nanoparticles through a cathepsin-sensitive linker. This is shown to increase stability and loading, thereby expanding the therapeutic window in multiple syngeneic tumour models, enabling the study of how the long-term fate of the nanoparticles affects the immune response. In a melanoma mouse model, primary tumour clearance depends on the STING signalling by host cells—rather than cancer cells—and immune memory depends on the spleen. The cancer cells act as a depot for the nanoparticles, releasing them over time to activate nearby immune cells to control tumour growth. Collectively, this work highlights the importance of nanoparticle structure and nano-biointeractions in controlling immunotherapy efficacy.

The stimulation of innate immune danger sensors, such as the cytosolic cyclic dinucleotide (CDN) sensor stimulator of interferon genes (STING), is a powerful therapeutic strategy to generate durable antitumour immune responses<sup>1–4</sup>. STING agonism enacts a type I interferon proinflammatory pathway that drives multifaceted antitumour immune functions in the tumour microenvironment (TME) and tumour-draining lymph nodes (tdLNs) by recruiting and activating immune cells<sup>5,6</sup> and enhancing natural killer (NK) cell<sup>7,8</sup> and T-cell-mediated tumour killing<sup>9,10</sup>. To achieve exogenous STING activation, small-molecule mimetics of CDNs have been synthesized<sup>11–13</sup>, leading to notable efficacy in preclinical models, which was further enhanced when combined with other therapeutic modalities<sup>14–16</sup>.

However, drug delivery challenges, including rapid clearance from the TME, poor cell internalization and systemic toxicity, have limited CDN efficacy in preclinical and clinical trials<sup>17,18</sup>.

Nanotechnology has been employed to address these challenges by altering the pharmacokinetics (PK), biodistribution (BD) and cytosolic delivery of CDN therapy, resulting in moderate effect in preclinical models<sup>19–21</sup>. However, these formulations relied on the encapsulation or electrostatic complexation of endogenous CDNs, such as cGAMP, raising issues regarding stability and potency following systemic administration *in vivo*. The design of more effective CDN nanoparticle (NP) formulations can be informed by examining the impact of NP-driven alterations in BD on drug pharmacodynamics (PD). Previous studies

<sup>1</sup>Institute for Medical Engineering and Science, Massachusetts Institute of Technology, Cambridge, MA, USA. <sup>2</sup>Department of Medicine, Division of Engineering in Medicine, Brigham and Women's Hospital, Harvard Medical School, Boston, MA, USA. <sup>3</sup>Wyss Institute for Biologically Inspired Engineering, Harvard University, Boston, MA, USA. <sup>4</sup>Harvard-MIT Division of Health Sciences & Technology, Massachusetts Institute of Technology, Cambridge, MA, USA. <sup>5</sup>Takeda Development Center Americas, Inc. (TDCA), Lexington, MA, USA. <sup>6</sup>Biodevek, Cambridge, MA, USA. ✉e-mail: [pdostapons@bwh.harvard.edu](mailto:pdostapons@bwh.harvard.edu); [nartzi@bwh.harvard.edu](mailto:nartzi@bwh.harvard.edu)

have explored the role of phagocytic immune cells in modulating NP penetration<sup>22</sup>, cellular distribution<sup>22,23</sup> and residence time<sup>23,24</sup> in the TME following extravasation. However, NPs are also uptaken by cancer cells<sup>23</sup> and although the co-localization of STING agonists with tumour antigens can stimulate a CD8<sup>+</sup> T-cell-mediated antitumour response<sup>25</sup>, STING activation in tumour cells does not directly contribute to therapeutic efficacy in most cancer types<sup>19,26</sup>. Consequently, in the context of immunotherapy, it is important to understand the fate of the NPs internalized by tumour cells. The high accumulation of immunotherapy-loaded NPs in reticuloendothelial organs after systemic delivery is believed to be a dose-limiting liability, hindering an optimal NP dose from reaching the TME<sup>27</sup>. Concurrently, the activation of antigen-presenting cells within these organs has been shown to contribute to CDN-NP efficacy<sup>8,28</sup>. Given the contributions of the spleen to peripheral immunity<sup>29,30</sup>, further work describing its contribution to the efficacy and mechanisms of NP-mediated CDN immunotherapy would be insightful.

Here we report the design of a highly potent drug-conjugated poly( $\beta$ -amino ester) (pBAE) NP formulation (CDN-NPs) for the intravenous (i.v.) delivery of STING agonists (Fig. 1a). The covalent conjugation of CDN to NPs led to a serum-stable formulation and sub-microgram doses of CDN-NPs in combination with immune checkpoint blockade (ICB) therapy induced robust tumour rejection and memory formation in multiple syngeneic murine cancer models. The extensive accumulation of CDN-NPs in the spleen motivated studying its role in generating antitumour efficacy. The treatment of splenectomized mice showed that this organ did not contribute to therapy efficacy against the primary tumour, but was responsible for the ability of the mice to reject tumours on rechallenge. We also show that CDN-NPs that were internalized by cancer cells were released over time and taken up by immune cells, inducing their STING-specific activation and restraining tumour growth (Fig. 1b). This novel CDN-conjugated NP reaffirms the therapeutic potential of systemic STING agonism and illustrates how NPs can be engineered to improve the pharmacological properties of CDNs, which directly impacts their antitumour efficacy.

## CDN-NPs increase immune cell activation compared with CDN-polyplexes

We previously used positively charged polypeptide-modified pBAEs (Supplementary Figs. 1–5) to electrostatically complex anionically charged gene therapies<sup>31–37</sup>. Here we tested the ability of those polymers to deliver CDNs and stimulate downstream STING activity via interferon regulatory factor 3 (IRF3) and NF- $\kappa$ B, using a reporter human monocyte THP1-Dual cell line. We found that the modification of pBAEs with positively charged arginine polypeptides (C6-CR3) complexed with negatively charged CDNs formed CDN-polyplexes, which elicited higher levels of IRF3 and NF- $\kappa$ B activation compared with free CDN (Supplementary Fig. 6). However, CDN-polyplexes lost their activity after incubation in physiological medium for 48 h,

limiting their clinical applicability (Supplementary Fig 7). To increase stability, we modified the CDN, STING agonist ML-317 (ref. 38), with a cathepsin-cleavable linker containing a terminal maleimide group<sup>39</sup> (Fig. 1a and Supplementary Fig. 8), allowing its covalent conjugation to the pBAE polymer. The CDN modification did not affect its *in vitro* activity compared with unmodified CDN (Supplementary Fig. 9). The cathepsin-cleavable linker was incorporated to facilitate the lysosomal proteolysis of the CDN into its free form within the cell via a two-step self-immolating process<sup>40</sup> (Supplementary Fig. 10). To conjugate the ML-317-linker to the pBAE polymer, acrylate groups were functionalized with 2-methyl-3-furanthiol (Supplementary Figs. 11 and 12), allowing a Diels–Alder reaction between the ML-317-linker maleimide group and polymer furan group<sup>41,42</sup>. The resultant NPs self-assembled to form conjugated CDN-NPs (Fig. 1a). NPs containing up to 3.1% (w/w) of ML-317-Linker-pBAE polymer were formed without compromising their stability (Supplementary Fig. 13). Finally, CDN-NPs were PEGylated to enhance their circulatory half-life<sup>43</sup> (Supplementary Figs. 14 and 15). CDN-NPs were 41 ± 5 nm in size and had a surface charge of +22 ± 3 mV (Fig. 1c). CDN release from CDN-NPs was quantified using liquid chromatography with tandem mass spectrometry (LC-MS/MS). CDN-NPs contained 18.1 ± 0.9  $\mu$ g CDN per mg polymer and the cathepsin linker was not affected by conjugation (Fig. 1d and Supplementary Fig. 16). We also confirmed that CDN-NPs are stable in mouse plasma for 24 h (Supplementary Fig. 17). CDN-NPs had quadruple the CDN content per particle compared with CDN-polyplex, resulting in greater cell tolerance towards CDN-NPs (Supplementary Fig. 18).

Then, we showed that CDN-NPs are efficiently internalized by immune cells via caveolin and clathrin endocytosis, with more than 90% uptake at 1 nM CDN (Supplementary Figs. 19–21), and the NPs underwent slow hydrolysis and disassembled at endosomal pH (Supplementary Figs. 22 and 23). We also showed that CDN-NPs resulted in markedly higher IRF3 activation compared with free CDN in THP1-Dual cells (half-maximum effective concentration (EC<sub>50</sub>) = 20.6 nM and 1,146.0 nM, respectively) (Fig. 1e) with a similar trend observed for the NF- $\kappa$ B response (Fig. 1f). In contrast, no activation of IRF3 or NF- $\kappa$ B was detected in STING KO THP1-Dual cells (Supplementary Fig. 24), confirming STING-specific activation. Similar results were obtained in bone-marrow-derived dendritic cells (BMDCs) and bone-marrow-derived macrophages (BMDMs) (Fig. 1g,h). Importantly, CDN-NPs remain active following 48 h of incubation in phosphate-buffered saline (PBS) (Fig. 1i), and can be stored for up to one month at 4 °C whilst maintaining their physicochemical properties and functionality (Supplementary Fig. 25).

## Immune cell uptake of CDN-NPs elicits robust cytokine production

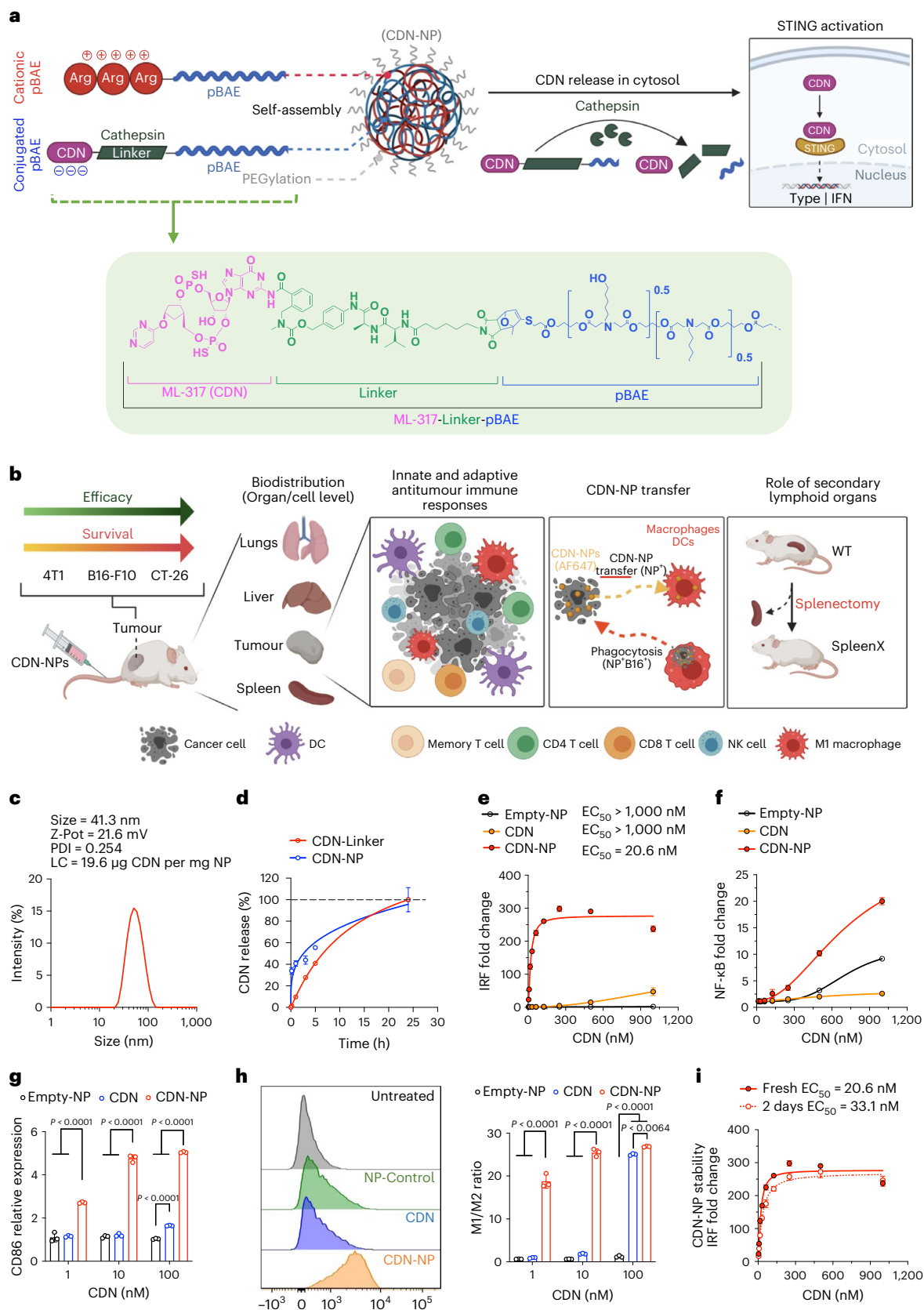
To evaluate the PK of CDN-NPs, B16-F10 melanoma tumour-bearing mice were injected i.v., and the concentration of CDN and polymer was

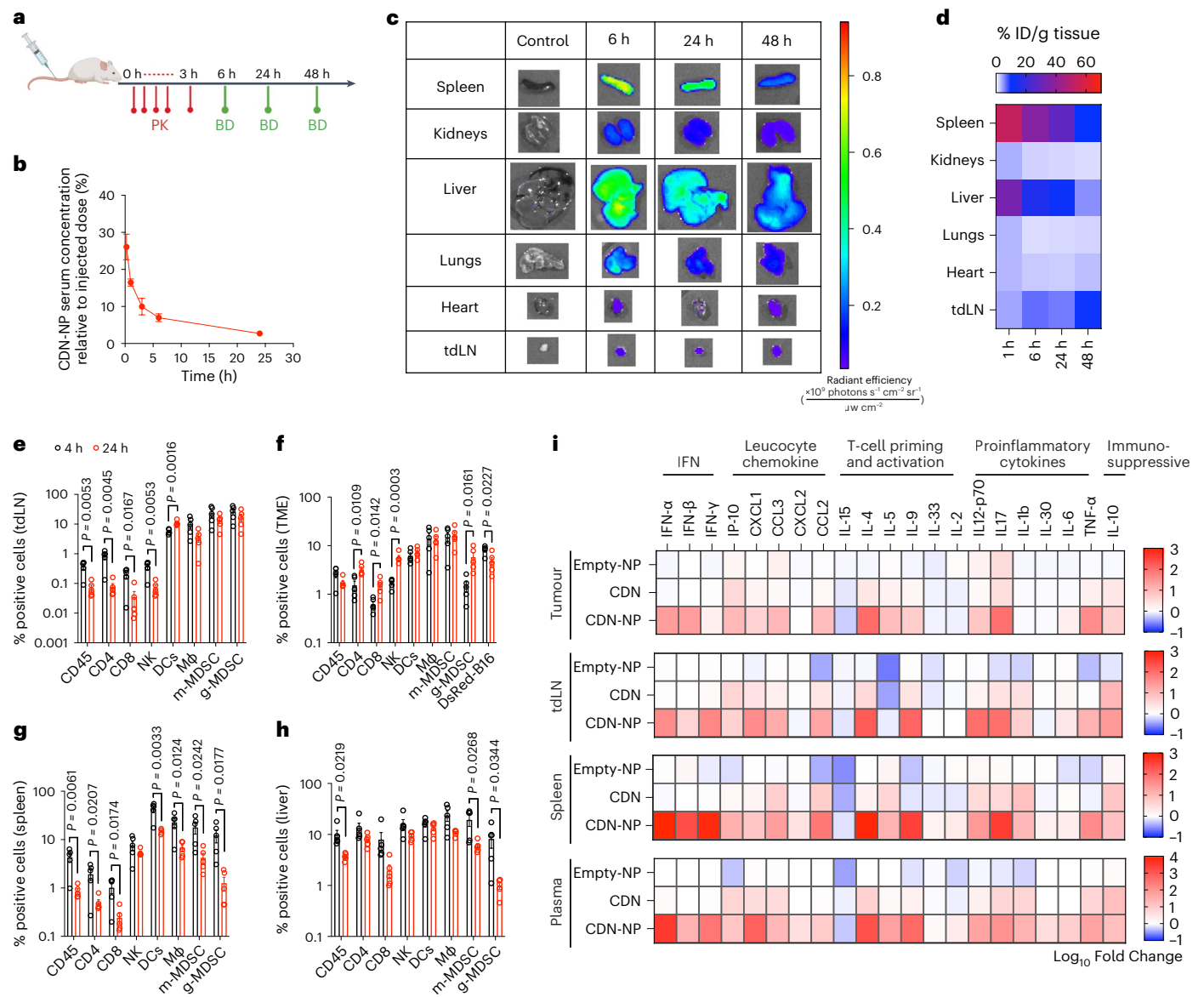
**Fig. 1 | Schematic, optimization and characterization of CDN-NP formulations.** **a**, Synthesis of CDN-conjugated NPs. Cationic pBAEs are formulated by mixing acrylate-terminate pBAE polymer with arginine-oligopeptide (termed C6-CR3). Maleimide-modified ML-317 is conjugated to pBAE by the Diels–Alder reaction (termed ML-317-Linker-pBAE). After CDN conjugation, ML-317-Linker-pBAE polymer is electrostatically complexed with C6-CR3 polymer, resulting in the formation of covalently conjugated CDN-NP. CDN-NPs are PEGylated using NHS-PEG and purified and sterilized by filtration. CDN is released from the CDN-NPs through a cathepsin-cleavable linker in the cell cytoplasm. **b**, Therapeutic efficacy of CDN-NPs was studied using different murine preclinical tumour models. We further investigated the role of cancer cells and host cells, particularly immune cells, in the context of CDN-NP therapeutic efficacy. **c**, Biophysical characterization of CDN-NPs was determined by dynamic light scattering. Representative data from three independent experiments with similar results are shown. **d**, To quantify the enzymatic cleavage rate of the CDN-cathepsin linker, CDN-NPs were incubated

with papain enzyme and the total CDN released was quantified at different time points by LC-MS/MS. **e**, Dose–response curves of the IRF response produced by CDN-NPs, Empty-NP or free CDN in the THP1-Dual cell line. **f**, Dose–response curves of the NF- $\kappa$ B response produced by CDN-NPs, Empty-NP or free CDN in the THP1-Dual cell line. **g**, Flow cytometric quantification of CD86 expression in DCs (CD86<sup>+</sup>CD11c<sup>+</sup>MHC-II<sup>+</sup>) 24 h following CDN-NP treatment at different CDN doses. **h**, Flow cytometry histogram (left; representative data from two independent experiments with  $n = 3$  are shown) and M1/M2 ratio (right) 24 h following CDN-NP treatment at different CDN doses. Inflammatory M1-like was defined by the CD86 expression and anti-inflammatory M2-like was defined by the CD206 expression. **i**, Comparison of IRF responses generated by fresh and 48 h incubated CDN-NPs in PBS. The data represent mean ± s.e.m., from a representative experiment of 2–3 independent experiments with  $n = 3$  (**d–i**) biologically independent samples. The data were analysed by two-way ANOVA with Bonferroni's multiple-comparisons tests (**g** and **h**). Panels **a** and **b** were created with BioRender.com.

quantified using LC-MS/MS and fluorescence respectively (Fig. 2a). We found that the CDN concentration in plasma was below the detection limit 15 minutes after i.v. administration of free CDN. In contrast, CDN derived from CDN-NPs was readily detected up to 1 h post-administration, with a plasma concentration of 50 nM (16.2 ± 0.5%

of the initial dose) (Supplementary Fig. 26). NP fluorescence in plasma 1 h following administration was 16.5 ± 1.7% of the initial injected NP dose, similar to that of the CDN, implying that the CDN-NP remains intact. Moreover, 2.7 ± 0.6% of the NPs were still detected in circulation 24 h post-administration (Fig. 2b).





**Fig. 2 | CDN-NP distribution, cell internalization and cytokine activation after i.v. administration.** **a**, Schematic of the timeline for PK and BD studies following CDN-NP systemic delivery in mice bearing B16-F10 tumours. **b**, PK analysis of fluorescent CDN-NPs upon i.v. administration. **c**, Representative IVIS images of organs. Distribution of total adjusted radiant efficiency within each time point in the spleen, kidneys, liver, lungs, heart, and tdLN. Representative data from two independent experiments with  $n = 4$  are shown. **d**, Fluorescent CDN-NP quantification in organs. **e–h**, Cellular internalization of fluorescent

CDN-NPs in different tissues: tdLN (**e**), tumour (**f**), spleen (**g**) and liver (**h**). **i**, Cytokine profile 4 h after the systemic administration of CDN-NP, NP control or free CDN in the tumour, spleen, tdLN and plasma. Values are represented as  $\log_{10}$  fold compared to untreated animals. Data are shown as mean  $\pm$  s.e.m. from two independent experiments with  $n = 3$  (**b**),  $n = 4–5$  (**d**) and  $n = 5$  (**e–i**) biologically independent samples. The data were analysed by Student's *t*-tests (**e–h**). Panel **a** was created with BioRender.com.

To characterize the BD of CDN-NPs, mice were injected i.v. with fluorescent formulations, and the organs were analysed at different time points. CDN-NPs were found to preferentially accumulate in the liver and spleen 6 h post-administration, which is consistent with the BD profile observed using arginine-modified pBAE NPs<sup>44</sup>. However, CDN-NP accumulation rapidly decreased in those organs 48 h post-administration, and was accompanied by a slight increase in the tdLN (Fig. 2c,d and Supplementary Fig. 27). Indeed, the size of CDN-NPs is highly consistent with hepatic or splenic tropism<sup>45,46</sup>. Finally, we quantified the CDN accumulation in the TME by LC-MS/MS as melanin was found to quench fluorescence. We found that a maximum of 4% of the administered CDN-NPs were retained in the TME 6 h post-administration, with 2% remaining after 48 h (Supplementary Fig. 28).

Next, we investigated the cellular distribution and accumulation of CDN-NPs in different organs (Fig. 2e–h). In the spleen, tdLN and tumour, NPs were principally internalized by dendritic cells (DCs), macrophages, granulocytic myeloid-derived suppressor cells (g-MDSC) and monocytic myeloid-derived suppressor cells (m-MDSC). In the spleen—and to a lesser extent, in the liver—the percentage of DCs and macrophages containing NPs (NP<sup>+</sup>) decreased at 24 h compared with 4 h. Interestingly, the converse was observed in the tdLN where an increase in DCs was observed at 24 h. A decrease in other myeloid populations was similarly seen 24 h after administration in the tdLN as was seen in the spleen and liver. Interestingly, we found that a high percentage of CDN-NPs that reach the TME are internalized by cancer cells, leading to  $8.2 \pm 1.7\%$  of cancer cells being NP<sup>+</sup> at 4 h and  $4.7 \pm 2.4\%$  at 24 h (Fig. 2f).

To understand how CDN-NP distribution and uptake by immune cells modulated the downstream inflammatory responses, we measured proinflammatory cytokines and chemokines in plasma, tdLN, TME and spleen (Fig. 2i and Supplementary Fig. 29), as these can trigger macrophage and DC maturation and CD8<sup>+</sup> T-cell cross-priming<sup>4</sup>. Compared with free CDN and NPs that did not contain CDN (Empty-NPs), CDN-NPs increased the expression of type I and type II interferons across all of the analysed tissues. Similar to our BD data, the highest interferon expression was observed in the spleen. Immunosuppressive IL-10 was also upregulated across all the tissues acting as an endogenous negative regulator of STING activation<sup>47</sup>. CDN-NP treatment also resulted in the elevated expression of proinflammatory cytokines, such as IL-17, IL-12-p70 and tumour necrosis factor alpha. CDN-NPs increased the expression of other cytokines involved in T-cell priming and activation such as IL-4 (ref. 48) and IL-9 (ref. 49) and increased expression of chemokines IP-10, CXCL1 CCL3 and CCL2 in the TME, which are critical for antitumour T-cell activation and immune cell recruitment<sup>50</sup>. The data suggest that immune cells in the secondary lymphoid organs (spleen) may play a role in the antitumour efficacy of CDN-NPs by priming T cells, secreting cytokines or facilitating cell migration to the tumour or tdLN.

### CDN-NPs induce a potent antitumour response in multiple tumour models

CDN conjugation to pBAE polymer increased the potency of the therapy, where a single dose of 1.25 µg CDN was the maximum tolerated dose (Supplementary Fig. 30). To ensure tolerability on repeated dosing, we selected a dose of 0.5 µg CDN, which showed transient body weight loss (Supplementary Fig. 31) and no toxicity in the liver and spleen (Supplementary Figs. 32 and 33). To evaluate the therapeutic efficacy of CDN-NPs in combination with ICB, we first utilized a poorly immunogenic murine melanoma model (B16-F10). CDN was administered i.v. seven days after tumour inoculation, with anti-PD-1 dosed intraperitoneally 24 h afterwards. This regimen was repeated three times every four days. CDN-NP therapy resulted in a substantial delay in tumour growth and a corresponding increase in mouse survival compared with free CDN, which resulted in a modest suppression of tumour growth and no increase in survival (Fig. 3a–c). Empty-NP treatment did not affect tumour growth (Supplementary Fig. 34). A slight benefit was observed when anti-PD-1 was combined with free CDN, but the combination of CDN-NP with anti-PD-1 markedly reduced tumour growth and 60% of the animals completely rejected tumours with no evidence of residual tumour two months post-treatment (Fig. 3a–c). These results confirm the synergistic effect of STING agonists and ICB<sup>51</sup>; however, this synergy was greatly accentuated using CDN-NPs.

To further explore the efficacy of CDN-NPs in models with differing biology, we next treated mice with colon (CT-26) and breast (4T1) tumours as CT-26 is more immunogenic than B16-F10 melanoma and 4T1 is poorly immunogenic and resistant to ICB<sup>52</sup>. In the CT-26 model, 30% of the tumour-bearing animals were cured with CDN-NP alone, and 70% showed complete tumour regression when combined with anti-PD-1 (Fig. 3d–f). A more restrained therapeutic response

was observed in mice bearing 4T1 tumours (Fig. 3g–i). CDN-NP treatment inhibited tumour growth and increased survival compared with free CDN, but no additional effect was observed when combined with anti-PD-1, for both CDN-NP and free CDN.

Following the rechallenge of cured mice (Fig. 3j), 60% (Fig. 3k) and 100% (Fig. 3l) of the mice rejected B16-F10 and CT-26 tumours, respectively, whereas all the age-matched naïve mice rapidly succumbed to their tumours. The combination of CDN-NP and anti-PD-1 generated a robust immune memory response in most initially cured mice, with slightly higher responsiveness in the CT-26 model<sup>52</sup>.

### Systemic delivery of CDN-NPs activates innate and adaptive immunity

To understand the mechanisms associated with CDN-NP antitumour activity, we analysed the innate and adaptive immune cell populations in the spleen, TME and tdLN of B16-F10 tumour-bearing mice two and seven days after therapy. The DC expression of CD86 in the tdLN and spleen was significantly increased (Fig. 4a), consistent with enhanced CDN accumulation delivered by CDN-NPs (Fig. 2d). The combination of ICB with CDN therapies further increased the CD86 expression on DCs compared with CDN monotherapy in the spleen. Interestingly, the combination of CDN-NP with anti-PD-1 significantly activated migratory (CD103<sup>+</sup>) and tissue-resident (CD8<sup>+</sup>) cross-presenting cDC1 subsets from the spleen, TME and tdLN (Supplementary Fig. 35 and Fig. 4b, respectively). The percentage of plasmacytoid DCs, which are known to produce high levels of type I interferons<sup>53</sup>, was increased in the spleen and TME after CDN-NP treatment (Supplementary Fig. 36). In contrast, the overall percentage of plasmacytoid DCs in the tdLN was decreased due to the influx of DCs after CDN-NP treatment.

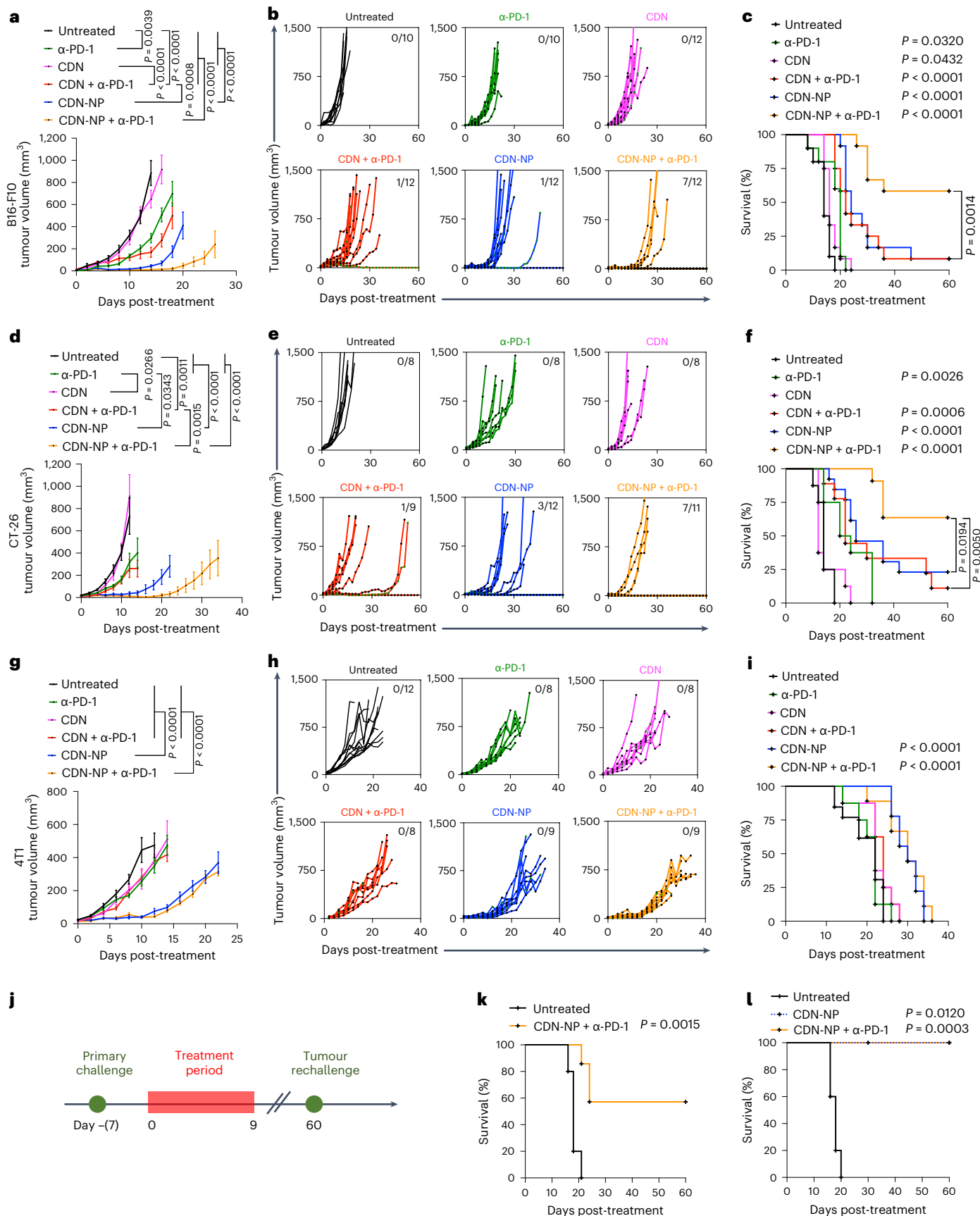
Furthermore, in the spleen and the tdLN, we observed the repolarization of M2-like macrophages (CD206<sup>hi</sup>) to a more M1-like state (CD86<sup>+</sup>) in mice treated with CDN-NPs alone or with ICB (Fig. 4c). CDN-NPs promoted an influx of g-MDSCs (CD45<sup>+</sup>CD11b<sup>+</sup>Ly6G<sup>+</sup>Ly6C<sup>low</sup>) to the TME and spleen (Supplementary Fig. 37a), a phenomenon that has previously been reported in response to STING-mediated inflammation<sup>54</sup>. Consequently, the percentage of m-MDSCs (CD45<sup>+</sup>CD11b<sup>+</sup>Ly6G<sup>+</sup>Ly6C<sup>high</sup>) was reduced in those tissues (Supplementary Fig. 37b). CDN-NPs also increased the proliferation (Ki67<sup>+</sup>) and activation of NK cells in the TME (Fig. 4d,e), which was encouraging given their role in STING-mediated immune responses, independent of CD8 T cells<sup>7</sup>.

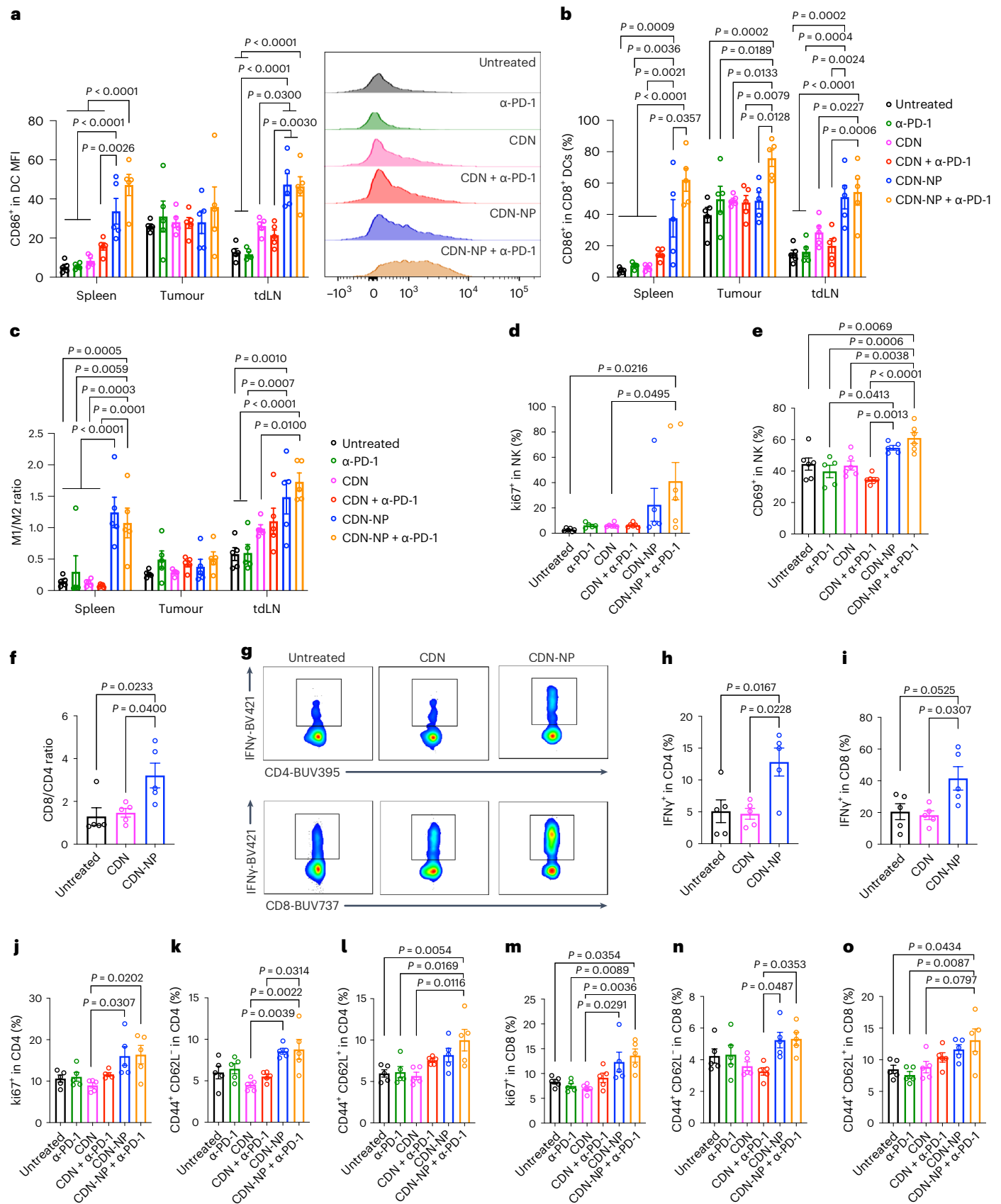
The analysis of tumour T cell infiltrates revealed a two-fold increase in the CD8/CD4 T cell ratio in the TME seven days post-CDN-NP treatment compared with equal doses of free CDN or untreated mice with a similar trend observed in the tdLN (Fig. 4f and Supplementary Fig. 38). Following ex vivo phorbol myristate acetate and ionomycin restimulation, we found that the proportion of CD4<sup>+</sup> T and CD8<sup>+</sup> T cells secreting IFN $\gamma$  in the TME was significantly increased in mice that were treated with CDN-NPs compared with the equivalent dose of free CDN or untreated mice (Fig. 4g–i). In line with their cytotoxic effector function, a higher percentage of IFN $\gamma$ -expressing cells were CD8<sup>+</sup> relative to CD4, which was also observed in the tdLN (Supplementary Fig. 39). In addition, the combined depletion of CD8<sup>+</sup> T cells, CD4<sup>+</sup> T cells and

#### Fig. 3 | CDN-NPs improve therapeutic outcome of CDN and synergize with ICB.

Mice with 30–50 mm<sup>3</sup> subcutaneous tumours were intravenously administered CDN-NPs, free CDN or PBS three times, four days apart. CDN therapy was combined with and without ICB, anti-PD-1, administered intraperitoneally (i.p.) 24 h after i.v. delivery of CDN, three times. **a**, Tumour growth in B16-F10 melanoma-bearing mice. **b, c**, Individual tumour growth curves (**b**) and Kaplan–Meier survival curves (**c**) of B16-F10 mice treated with different therapeutic combinations. **d**, Tumour growth in CT-26 colon tumour-bearing mice. **e, f**, Individual tumour growth curves (**e**) and Kaplan–Meier survival curves (**f**) of CT-26 tumour-bearing mice treated with different therapeutic combinations. **g**, Tumour growth in 4T1 triple-negative breast tumour-bearing mice. **h, i**, Individual tumour growth curves (**h**) and Kaplan–Meier survival curves (**i**) of

4T1 tumour-bearing mice treated with different therapeutic combinations. **j**, Rechallenge scheme of cured B16-F10 and CT-26 tumour-bearing mice. Cured mice were injected with  $5 \times 10^5$  B16-F10 or  $1 \times 10^5$  CT-26 cells in the opposite side of the flank at day 60 post-initial treatment. Tumour growth and survival were monitored. **k**, Kaplan–Meier survival curves of B16-F10 tumour-bearing mice. **l**, Kaplan–Meier survival curves of CT-26 tumour-bearing mice. The data are represented as mean  $\pm$  s.e.m. from a representative experiment of two independent experiments with  $n = 8–12$  (**a–i**) and  $n = 5–7$  (**k** and **l**) biologically independent samples. The data were analysed by two-way ANOVA with Bonferroni's multiple-comparisons tests (**a**, **d** and **g**) or log-rank (Mantel–Cox) test (**c**, **f**, **i**, **k** and **l**). The statistical significance was determined against an untreated group unless indicated otherwise by the Mantel–Cox test (**c**, **f**, **i**, **k** and **l**).





NK cells resulted in a complete loss of CDN-NP-mediated antitumour activity (Supplementary Fig. 40).

We next investigated whether T cell memory had been formed in the tdLN, seven days after a single treatment. We observed an increase

in CD4 and CD8 T cell proliferation (ki67<sup>+</sup>) and activation (CD69<sup>+</sup>) after CDN-NP treatment compared with untreated or free CDN groups (Fig. 4j,m and Supplementary Fig. 41, respectively). Interestingly, the percentages of CD4<sup>+</sup>CD44<sup>hi</sup>CD62L<sup>hi</sup> central memory T cells (T<sub>CM</sub>) and

**Fig. 4 | CDN-NPs activate innate and adaptive antitumour immune responses.**

Free CDN or CDN-NPs (0.5 µg) alone or in combination with anti-PD-1 (100 µg) were administered seven days after tumour inoculation (average tumour volume, ~30–50 mm<sup>3</sup>). B16-F10 tumours, tdLN and spleen were collected and analysed two days and/or seven days after treatment. **a**, Quantification of activated DCs (CD86<sup>hi</sup>CD11c<sup>+</sup>MHCII<sup>+</sup>CD45<sup>+</sup>) in the spleen, TME and tdLN (left) and representative flow cytometry histograms in the spleen (right; representative data from two independent experiments with  $n = 5$  are shown) two days following i.v. injection. **b**, Representative flow quantification of activated resident DCs (CD86<sup>hi</sup>CD8<sup>+</sup>CD11c<sup>+</sup>MHCII<sup>+</sup>CD45<sup>+</sup>) in the spleen, TME and tdLN two days following i.v. injection. **c**, Relative quantification of M1-like macrophages (CD86<sup>hi</sup>) and M2-like macrophages (CD206<sup>hi</sup>) ratio gating on F4/80<sup>+</sup>CD11b<sup>+</sup>CD45<sup>+</sup> cells in the spleen, TME and tdLN two days following i.v. injection. **d, e**, NK cell proliferation (ki67<sup>+</sup>NK1.1<sup>+</sup>) (**d**) and activation (CD69<sup>+</sup>NK1.1<sup>+</sup>) (**e**) in the TME were quantified by flow cytometry seven days following i.v. injection. **f**, Ratio of

CD8<sup>+</sup> to CD4<sup>+</sup> T cells in the TME at two and seven days following treatment. **g–i**, Representative flow cytometric analysis images (**g**) and the relative quantifications of IFNγ<sup>+</sup>CD4<sup>+</sup> (**h**) and IFNγ<sup>+</sup>CD8<sup>+</sup> (**i**) T cells in the TME seven days after i.v. injection. **j**, CD4 cell proliferation (ki67<sup>+</sup>CD4<sup>+</sup>CD3<sup>+</sup>) in the tdLN was quantified by flow cytometry seven days following i.v. injection. **k, l**, Central CD4<sup>+</sup> cell memory (CD44<sup>+</sup>CD62L<sup>+</sup>) (**k**) and effector CD4<sup>+</sup> cell memory (CD44<sup>+</sup>CD62L<sup>-</sup>) (**l**) in the tdLN seven days following treatment. **m**, CD8 cell proliferation (ki67<sup>+</sup>CD8<sup>+</sup>CD3<sup>+</sup>) in the tdLN was quantified by flow cytometry seven days following i.v. injection. **n, o**, Central CD8<sup>+</sup> cell memory (CD44<sup>+</sup>CD62L<sup>+</sup>) (**n**) and effector CD8<sup>+</sup> cell memory (CD44<sup>+</sup>CD62L<sup>-</sup>) (**o**) in the tdLN seven days following treatment. The data are represented as mean ± s.e.m. from a representative experiment of two independent experiments with  $n = 5$  (**a–c**, **f** and **h–o**) and  $n = 5–6$  (**d** and **e**) biologically independent samples. The data were analysed by two-way ANOVA (**a–c**) or one-way ANOVA (**d–f** and **h–o**) with Bonferroni's multiple-comparisons tests.

CD4<sup>+</sup>CD44<sup>hi</sup>CD62L<sup>lo</sup> effector memory T cells (T<sub>EM</sub>) were both increased in CDN-NP-treated mice (Fig. 4k, l). A similar profile was found in CD8<sup>+</sup> T cells, where CDN-NP-treated mice with anti-PD-1 showed higher percentages of T<sub>CM</sub> and T<sub>EM</sub> cells compared with untreated and free CDN groups (Fig. 4n, o). These results provide evidence that treatment with CDN-NPs most effectively promotes the generation of immune memory cell populations, contributing to the differences seen among these treatments.

**STING activation in host rather than cancer cells drives efficacy**

To investigate the role of host cell versus cancer cell STING in generating antitumour efficacy, STING KO (M<sup>-/-</sup>) or wild-type (M<sup>wt</sup>) mice were inoculated with either wild-type (T<sup>wt</sup>) or STING KO (T<sup>-/-</sup>) B16-F10 tumour cells (Fig. 5a). Treatment with CDN-NPs in M<sup>wt</sup>T<sup>wt</sup> mice resulted in an inhibition of tumour growth (Fig. 5b, c) and a significant increase in overall survival (Fig. 5d) compared with the corresponding untreated mice. Similar results were obtained when M<sup>wt</sup>T<sup>-/-</sup> mice were treated with CDN-NPs, whereas the therapeutic efficacy of CDN-NPs in T<sup>wt</sup> or T<sup>-/-</sup> tumour-bearing M<sup>-/-</sup> mice was completely abolished. These results confirm that CDN-NP elicits tumour regression through the activation of host cell STING.

**Splenectomized mice show compromised long-term memory**

Given the robust accumulation of CDN-NPs in the spleen and the activation of splenic immune cell populations, we investigated the contribution of the spleen to the generation of antitumour efficacy. We induced B16-F10 tumours in splenectomized mice (SpleenX) and treated them as previously described (Fig. 5e). We found that the absence of spleen did not have any bearing on the ability of mice to reject their primary tumours when treated with CDN-NP alone and in combination with ICB (Fig. 5f–g). However, only wild-type (WT) mice were able to reject the tumour upon rechallenge (Fig. 5h). We found no significant differences in innate immune cell populations between WT and SpleenX models

(Supplementary Figs. 42 and 43). However, compared with WT animals, SpleenX mice had half the number of lymphocytes in the tdLN (Fig. 5i) with a notable reduction in CD4<sup>+</sup> T cells in the tdLN (Supplementary Fig. 44). Interestingly, activated CD4<sup>+</sup> T cells from the spleen or tdLN have been shown to confer potent antitumour protection<sup>55</sup>, and are known to participate in the generation of functional immune memory<sup>56</sup>. The lack of a spleen seems to have been compensated for by an increase in the activation of CD8<sup>+</sup> T cells in the tdLN of the splenectomized mice (Supplementary Fig. 45).

**CDN-NPs released from cancer cells activate proximal immune cells**

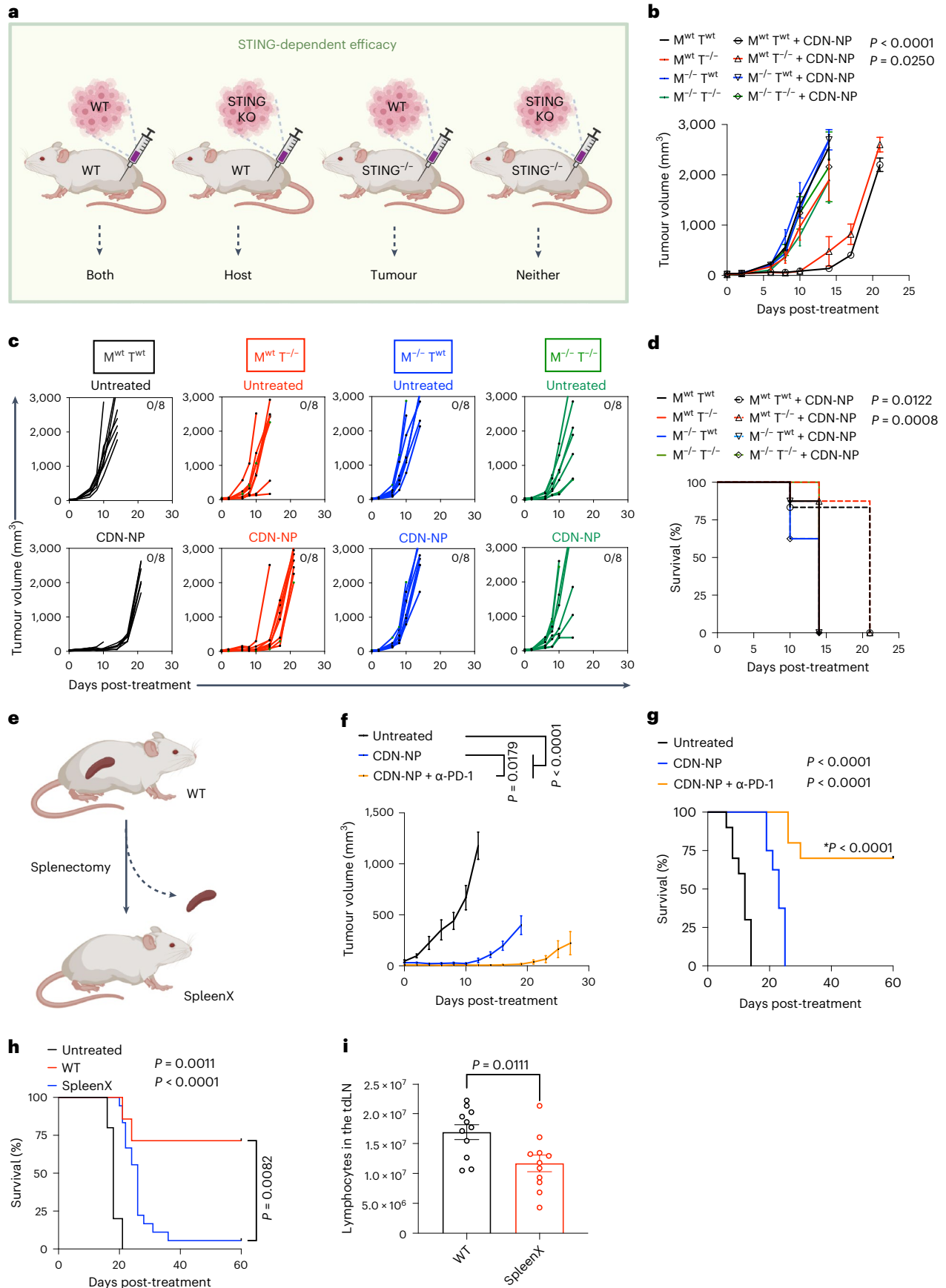
As cancer cell STING activation did not contribute to the therapeutic efficacy (Fig. 5a–d) but are a considerable recipient of the therapy (Fig. 2f), we sought to resolve the fate of CDN-NPs that have entered cancer cells. Interestingly, cancer cells can produce CDNs that are transferred to tumour-associated DCs and macrophages, inducing type I interferon production<sup>57,58</sup>. We hypothesized that cancer cells can act as a reservoir for CDN-NPs, releasing CDN-NPs to tumour-resident DCs and macrophages over time (Fig. 6a). To investigate this phenomenon, we first confirmed that CDN-NPs preloaded into cancer cells (Supplementary Fig. 46) are released over time in vitro. Cancer cells were treated with 1 µM CDN-NPs to ensure cell viability (IC<sub>50</sub>, 15 µM) (Supplementary Fig. 47). We found that CDN-NPs were gradually released from cancer cells within the first 8 h and almost completely released by 48 h (Fig. 6b). We confirmed the presence of CDN-NPs in THP1 and RAW cell lines when co-cultured for 24 h with tumour cells that were pretreated with CDN-NPs or free CDN at equivalent doses (Fig. 6c). We found that IRF3 was activated in STING WT THP1 (THP1<sup>wt</sup>) and RAW (RAW<sup>wt</sup>) cells, but not in STING KO THP1 (THP1<sup>-/-</sup>) or RAW (RAW<sup>-/-</sup>) cells, when co-cultured with tumour cells (either STING WT (B16<sup>wt</sup>) or STING KO (B16<sup>-/-</sup>) cells) that were pretreated with CDN-NPs (Fig. 6d). A similar trend was obtained using STING WT BMDCs (DC<sup>wt</sup>) and BMDMs (Mφ<sup>wt</sup>), where an increase in activated CD86<sup>+</sup> cells was observed when cancer cells were pretreated with

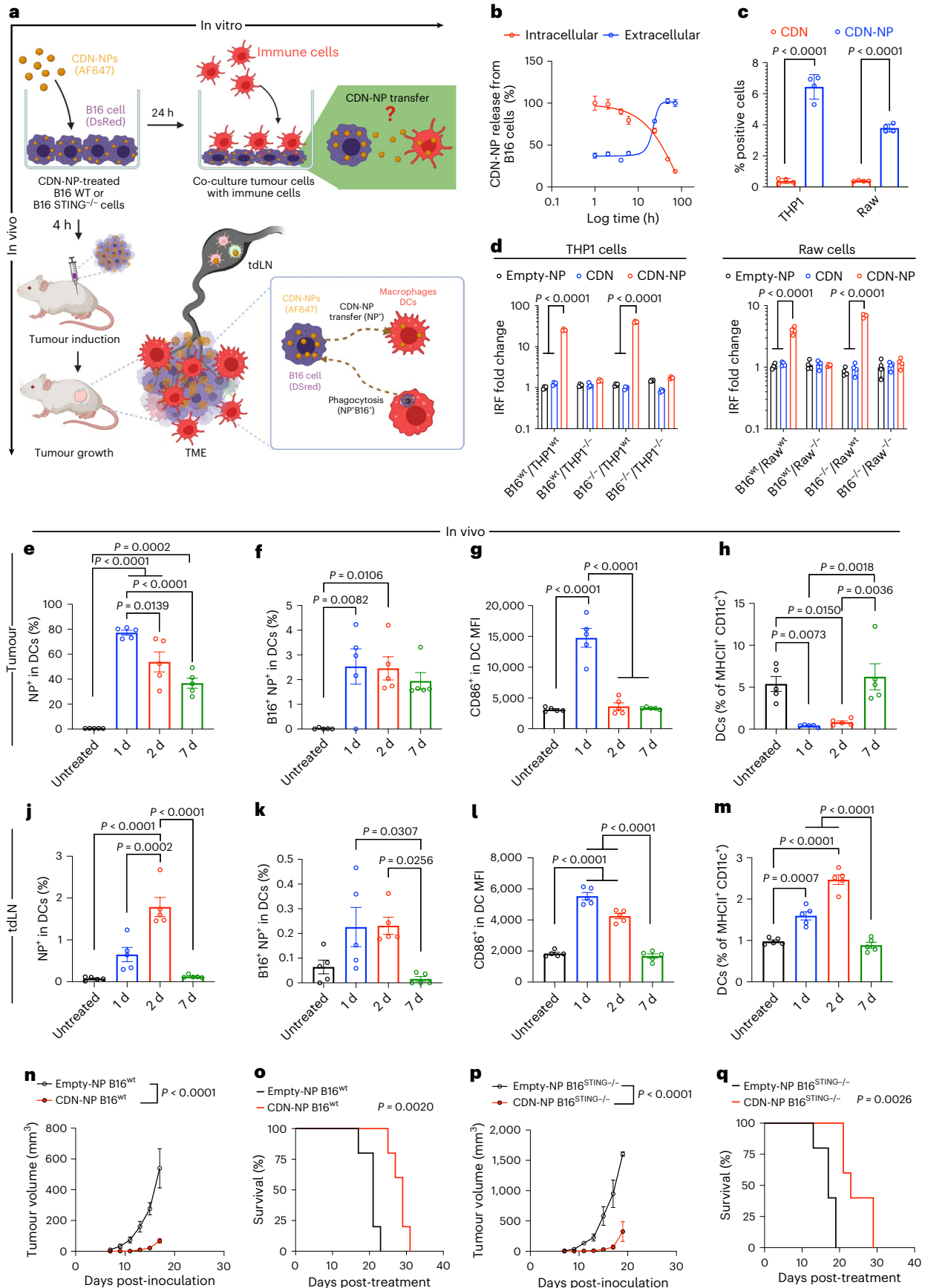
**Fig. 5 | Host cell activation following STING delivery is sufficient to promote antitumour immunity.**

**a**, Treatment scheme for the confirmation of CDN STING-dependent efficacy in the B16-F10 melanoma model. B16-F10 STING<sup>-/-</sup> or B16-F10 WT tumour cells were implanted in C57BL/6 STING<sup>-/-</sup> or C57BL/6 WT mice following CDN-NP treatment when the tumour size reached 30–50 mm<sup>3</sup>. **b**, Average tumour growth kinetics after treatment. **c**, Individual tumour growth curves. **d**, Kaplan–Meier survival curves. **e**, Role of spleen in CDN-NP therapy. Mice were subjected to splenectomy one week before tumour induction. Then, mice with 30–50 mm<sup>3</sup> subcutaneous tumours were treated with CDN-NPs (0.5 µg) with and without anti-PD-1 (100.0 µg). CDN therapy was intravenously administered three times, four days apart. The anti-PD-1 therapy was intraperitoneally administered 24 h after CDN treatment. **f**, Tumour

growth in B16-F10 melanoma-bearing mice. **g**, Kaplan–Meier survival curves. **h**, Rechallenge of cured WT and SpleenX B16-F10 tumour-bearing mice. Cured mice were injected with 5 × 10<sup>3</sup> B16-F10 on the opposite side of the flank at day 60 post-first treatment. Kaplan–Meier survival curves of B16-F10 tumour-bearing mice. **i**, Total lymphocyte count in tdLN tissues two days post-treatment. The data are represented as mean ± s.e.m. from a representative experiment of two independent experiments with  $n = 7–8$  (**b–d**),  $n = 8–10$  (**f–h**) and  $n = 11$  (**i**) biologically independent samples. The data were analysed by two-way ANOVA with Bonferroni's multiple-comparisons tests (**b** and **f**), log-rank (Mantel–Cox) test (**d**, **g** and **h**) or Student's *t*-test (**i**). The statistical significance was determined against the untreated group unless indicated otherwise by the Mantel–Cox test (**c**, **d**, **g** and **h**). Panels **a** and **e** were created with BioRender.com.







**Fig. 6 | Cancer cells serve as a CDN-NP reservoir, releasing the CDN-NPs into neighbouring immune cells and activating them.** **a**, Scheme of B16-F10 cancer cells acting as a reservoir of CDN-NPs, releasing them over time into neighbouring DCs or macrophages both in vitro and in vivo. To study this phenomenon, B16-F10 and DsRed-B16 cells were preloaded with CDN-NPs at 1,000 nM for 4 h. Then, CDN-NP-loaded cancer cells were co-cultured with different immune cells in vitro or subcutaneously injected in vivo. CDN-NP transfer to immune cells was studied by flow cytometry. **b**, CDN-NP release kinetics from B16-F10 cancer cells preloaded with CDN-NPs. Intracellular and released CDN-NPs were quantified at different time points by LC-MS/MS. **c**, Percentage of immune cells containing CDN-NPs transferred from cancer cells after 24 h of co-culture in vitro. **d**, IRF3 response produced by the transferred CDN-containing NPs or free CDN from B16<sup>wt</sup> or B16<sup>-/-</sup> to THP1<sup>wt</sup> or THP1<sup>-/-</sup> and RAW<sup>wt</sup> or RAW<sup>-/-</sup>. **e–m**, In vivo CDN-NP transfer from DsRed-B16 cancer cells to DCs. Percentage of CDN-NP-positive (NP<sup>+</sup>) DCs in the tumour (**e**). Percentage of

NP<sup>+</sup> and DsRed-B16-positive (B16<sup>+</sup>) DCs in the tumour (**f**). CD86 activation marker in the DCs present in the tumour (**g**). Total percentage of DCs in the tumour (**h**). Percentage of NP<sup>+</sup> DCs in the tdLN (**j**). Percentage of NP<sup>+</sup> and B16<sup>+</sup> DCs in the tdLN (**k**). CD86 activation marker in the DCs present in the tdLN (**l**). Total percentage of DCs in the tdLN (**m**). **n–q**, Tumour growth and survival using CDN-NPs or Empty-NP-treated (**n** and **o**) B16-F10 WT (B16<sup>wt</sup>) and (**p** and **q**) B16-F10 STING KO (B16<sup>-/-</sup>) cells. The data are represented as mean ± s.e.m. from a representative experiment of two independent experiments with  $n = 6$  (**b**),  $n = 4$  (**c** and **d**),  $n = 5$  (**e–l**) and  $n = 5$  (**m–p**) biologically independent samples. The data were analysed by two-way ANOVA (**c**, **d**, **m** and **o**) or one-way ANOVA (**e–l**) with Bonferroni's multiple-comparisons tests, or log-rank (Mantel–Cox) test (**n** and **p**). The statistical significance was determined against the untreated group unless indicated otherwise by Mantel–Cox test (**n** and **p**). Panel **a** was created with BioRender.com.

CDN-NPs. No increase in CD86 was observed in STING KO DCs (DC<sup>-/-</sup>) or macrophages (Mφ<sup>-/-</sup>) (Supplementary Fig. 48). These in vitro results illustrate that CDN-NPs released by cancer cells can activate the STING pathway in immune cells, acting as a reservoir of CDN-NPs. To confirm this in vivo, we used an engineered model where fluorescent CDN-NPs were preloaded into fluorescent cancer cells (DsRed-B16) before tumour inoculation, and the presence of fluorescent CDN-NPs and cancer cells in immune cells was evaluated. We found that 80% of DCs and 40% of macrophages in the TME were positive for CDN-NPs (NP<sup>+</sup>) 24 h after tumour inoculation (Fig. 6e and Supplementary Fig. 49a, respectively). To test whether this was a result of phagocytosis of cancer cells containing CDN-NPs by immune cells, rather than the release of CDN-NPs from cancer cells, we quantified the co-localization of fluorescent CDN-NPs and fluorescent cancer cells (DsRed-B16) in immune cells. The obtained results showed a low co-localization percentage (<3% for DCs and <2% for Mφ), indicating that phagocytosis alone did not explain CDN-NP presence in immune cells (Fig. 6f and Supplementary Fig. 49b). CDN-NP transfer and activation of DCs and macrophages in the TME after 24 h (Fig. 6g and Supplementary Fig. 49c) led to their migration to tdLN at 48 h (Fig. 6h, j and Supplementary Fig. 49d, h). This resulted in an increase in NP<sup>+</sup> DCs and macrophages in the tdLN and an increase in CD86 (Fig. 6i–k and Supplementary Fig. 49e–g). Finally, to investigate the contribution to therapeutic efficacy, both WT B16-F10 (B16<sup>wt</sup>) and STING KO B16-F10 (B16<sup>-/-</sup>) cells were incubated with CDN-NPs or Empty-NPs 4 h before tumour inoculation. CDN-NP-treated B16<sup>wt</sup> cells resulted in a delay in tumour growth and improved survival compared with Empty-NP-treated cells in WT C57BL/6 mice (Fig. 6n, o). Similar results were obtained with CDN-NP-treated B16<sup>-/-</sup> cells (Fig. 6p, q), confirming that tumour cell STING did not drive tumour growth inhibition and transferred CDN-NPs activated the STING pathway in host immune cells.

## Conclusions

This work establishes CDN-NPs as a potent innate immune agonist therapy. The conjugation of CDN to NPs ensures particle-dependent drug BD, resulting in superior potency, drug loading and stability compared with electrostatic NPs. When combined with ICB, low-dose CDN-NPs generated complete and durable antitumour responses and immunological memory in murine melanoma and colon cancer models. CDN-NPs were taken up by immune cells in the TME and secondary lymphoid organs. We discovered that CDN-NPs internalized by cancer cells were transferred to proximal immune cells in the TME. NPs also accumulate in the spleen, which contributed to immune memory formation. Rational engineering allowed us to define the NP fate, understand the mechanism of action and expand the therapeutic window. Finally, these findings underscore the importance of studying the temporal interplay between immune cell composition and activity, and the dynamic distribution of therapeutic NPs across organs and cell types, to inform the design of effective NP immunotherapies.

## Online content

Any methods, additional references, Nature Portfolio reporting summaries, source data, extended data, supplementary information, acknowledgements, peer review information; details of author contributions and competing interests; and statements of data and code availability are available at <https://doi.org/10.1038/s41565-023-01447-7>.

## References

1. Yum, S., Li, M., Frankel, A. E. & Chen, Z. J. Roles of the cGAS-STING pathway in cancer immunosurveillance and immunotherapy. *Annu. Rev. Cancer Biol.* **3**, 323–344 (2019).
2. Kwon, J. & Bakhom, S. F. The cytosolic DNA-sensing cGAS–STING pathway in cancer. *Cancer Discov.* **10**, 26 (2020).
3. Ishikawa, H., Ma, Z. & Barber, G. N. STING regulates intracellular DNA-mediated, type I interferon-dependent innate immunity. *Nature* **461**, 788–792 (2009).
4. Barber, G. N. STING: infection, inflammation and cancer. *Nat. Rev. Immunol.* **15**, 760–770 (2015).
5. Zitvogel, L., Galluzzi, L., Kepp, O., Smyth, M. J. & Kroemer, G. Type I interferons in anticancer immunity. *Nat. Rev. Immunol.* **15**, 405–414 (2015).
6. Woo, S.-R. et al. STING-dependent cytosolic DNA sensing mediates innate immune recognition of immunogenic tumors. *Immunity* **41**, 830–842 (2014).
7. Nicolai, C. J. et al. NK cells mediate clearance of CD8<sup>+</sup> T cell-resistant tumors in response to STING agonists. *Sci. Immunol.* **5**, eaaz2738 (2020).
8. Nakamura, T. et al. STING agonist loaded lipid nanoparticles overcome anti-PD-1 resistance in melanoma lung metastasis via NK cell activation. *J. Immunother. Cancer* **9**, e002852 (2021).
9. Fu, J. et al. STING agonist formulated cancer vaccines can cure established tumors resistant to PD-1 blockade. *Sci. Transl. Med.* **7**, 283ra252 (2015).
10. Dosta, P. et al. Delivery of stimulator of interferon genes (STING) agonist using polypeptide-modified dendrimer nanoparticles in the treatment of melanoma. *Adv. NanoBiomed Res.* **1**, 2100006 (2021).
11. Ablasser, A. et al. cGAS produces a 2'-5'-linked cyclic dinucleotide second messenger that activates STING. *Nature* **498**, 380–384 (2013).
12. Wu, J. et al. Cyclic GMP-AMP is an endogenous second messenger in innate immune signaling by cytosolic DNA. *Science* **339**, 826–830 (2013).
13. Zhang, X. et al. Cyclic GMP-AMP containing mixed phosphodiester linkages is an endogenous high-affinity ligand for STING. *Mol. Cell* **51**, 226–235 (2013).
14. Lee, S. E. et al. Improvement of STING-mediated cancer immunotherapy using immune checkpoint inhibitors as a game-changer. *Cancer Immunol. Immunother.* **71**, 3029–3042 (2022).

15. Jneid, B. et al. Selective STING stimulation in dendritic cells primes antitumor T cell responses. *Sci. Immunol.* **8**, eabn6612 (2023).
16. Wang, H. et al. cGAS is essential for the antitumor effect of immune checkpoint blockade. *Proc. Natl Acad. Sci. USA* **114**, 1637–1642 (2017).
17. Meric-Bernstam, F. et al. Phase Ib study of MIW815 (ADU-S100) in combination with spartalizumab (PDR001) in patients (pts) with advanced/metastatic solid tumors or lymphomas. *J. Clin. Oncol.* **37**, 2507 (2019).
18. Harrington, K. J. et al. Preliminary results of the first-in-human (FIH) study of MK-1454, an agonist of stimulator of interferon genes (STING), as monotherapy or in combination with pembrolizumab (pembro) in patients with advanced solid tumors or lymphomas. *Ann. Oncol.* **29**, VIII712 (2018).
19. Shae, D. et al. Endosomolytic polymersomes increase the activity of cyclic dinucleotide STING agonists to enhance cancer immunotherapy. *Nat. Nanotechnol.* **14**, 269–278 (2019).
20. Watkins-Schulz, R. et al. A microparticle platform for STING-targeted immunotherapy enhances natural killer cell- and CD8<sup>+</sup> T cell-mediated anti-tumor immunity. *Biomaterials* **205**, 94–105 (2019).
21. Koshy, S. T., Cheung, A. S., Gu, L., Graveline, A. R. & Mooney, D. J. Liposomal delivery enhances immune activation by STING agonists for cancer immunotherapy. *Adv. Biosyst.* **1**, 1600013 (2017).
22. Lin, Z. P. et al. Macrophages actively transport nanoparticles in tumors after extravasation. *ACS Nano* **16**, 6080–6092 (2022).
23. Miller, M. A. et al. Tumour-associated macrophages act as a slow-release reservoir of nano-therapeutic Pt(IV) pro-drug. *Nat. Commun.* **6**, 8692 (2015).
24. Korangath, P. et al. Nanoparticle interactions with immune cells dominate tumor retention and induce T cell-mediated tumor suppression in models of breast cancer. *Sci. Adv.* **6**, eaay1601 (2020).
25. Dane, E. L. et al. STING agonist delivery by tumour-penetrating PEG-lipid nanodiscs primes robust anticancer immunity. *Nat. Mater.* **21**, 710–720 (2022).
26. Sun, X. et al. Amplifying STING activation by cyclic dinucleotide-manganese particles for local and systemic cancer metalloimmunotherapy. *Nat. Nanotechnol.* **16**, 1260–1270 (2021).
27. Riley, R. S., June, C. H., Langer, R. & Mitchell, M. J. Delivery technologies for cancer immunotherapy. *Nat. Rev. Drug Discov.* **18**, 175–196 (2019).
28. Wehbe, M. et al. Nanoparticle delivery improves the pharmacokinetic properties of cyclic dinucleotide STING agonists to open a therapeutic window for intravenous administration. *J. Control. Release* **330**, 1118–1129 (2021).
29. Lewis, S. M., Williams, A. & Eisenbarth, S. C. Structure and function of the immune system in the spleen. *Sci. Immunol.* **4**, eaau6085 (2019).
30. Bronte, V. & Pittet, Mikael J. The spleen in local and systemic regulation of immunity. *Immunity* **39**, 806–818 (2013).
31. Segovia, N., Dosta, P., Cascante, A., Ramos, V. & Borrós, S. Oligopeptide-terminated poly( $\beta$ -amino ester)s for highly efficient gene delivery and intracellular localization. *Acta Biomater.* **10**, 2147–2158 (2014).
32. Dosta, P., Ramos, V. & Borrós, S. Stable and efficient generation of poly( $\beta$ -amino ester)s for RNAi delivery. *Mol. Syst. Des. Eng.* **3**, 677–689 (2018).
33. Dosta, P. et al. Delivery of anti-microRNA-712 to inflamed endothelial cells using poly(beta-amino ester) nanoparticles conjugated with VCAM-1 targeting peptide. *Adv. Healthcare Mater.* **10**, 2001894 (2021).
34. Nunez-Toldra, R. et al. Improvement of osteogenesis in dental pulp pluripotent-like stem cells by oligopeptide-modified poly(beta-amino ester)s. *Acta Biomater.* **53**, 152–164 (2017).
35. Dosta, P. et al. Delivery of siRNA to endothelial cells in vivo using lysine/histidine oligopeptide-modified poly(beta-amino ester) nanoparticles. *Cardiovasc. Eng. Technol.* **12**, 114–125 (2021).
36. Dosta, P., Segovia, N., Cascante, A., Ramos, V. & Borrós, S. Surface charge tunability as a powerful strategy to control electrostatic interaction for high efficiency silencing, using tailored oligopeptide-modified poly(beta-amino ester)s (PBAEs). *Acta Biomater.* **20**, 82–93 (2015).
37. Puigmal, N., Ramos, V., Artzi, N. & Borrós, S. Poly( $\beta$ -amino ester) s-based delivery systems for targeted transdermal vaccination. *Pharmaceutics* **15**, 1262 (2023).
38. Vyskocil, S. et al. Identification of novel carbocyclic pyrimidine cyclic dinucleotide STING agonists for antitumor immunotherapy using systemic intravenous route. *J. Med. Chem.* **64**, 6902–6923 (2021).
39. Alouane, A., Labruère, R., Le Saux, T., Schmidt, F. & Jullien, L. Self-immolative spacers: kinetic aspects, structure–property relationships, and applications. *Angew. Chem. Int. Ed.* **54**, 7492–7509 (2015).
40. Bargh, J. D., Isidro-Llobet, A., Parker, J. S. & Spring, D. R. Cleavable linkers in antibody–drug conjugates. *Chem. Soc. Rev.* **48**, 4361–4374 (2019).
41. Gandini, A. The furan/maleimide Diels–Alder reaction: a versatile click–unlick tool in macromolecular synthesis. *Prog. Polym. Sci.* **38**, 1–29 (2013).
42. Froidevaux, V. et al. Study of the Diels–Alder and retro-Diels–Alder reaction between furan derivatives and maleimide for the creation of new materials. *RSC Adv.* **5**, 37742–37754 (2015).
43. Harris, J. M. & Chess, R. B. Effect of pegylation on pharmaceuticals. *Nat. Rev. Drug Discov.* **2**, 214–221 (2003).
44. Fornaguera, C. et al. mRNA delivery system for targeting antigen-presenting cells in vivo. *Adv. Healthcare Mater.* **7**, 1800335 (2018).
45. Blanco, E., Shen, H. & Ferrari, M. Principles of nanoparticle design for overcoming biological barriers to drug delivery. *Nat. Biotechnol.* **33**, 941–951 (2015).
46. Cheng, Q. et al. Selective organ targeting (SORT) nanoparticles for tissue-specific mRNA delivery and CRISPR–Cas gene editing. *Nat. Nanotechnol.* **15**, 313–320 (2020).
47. Akdis, C. A. & Blaser, K. Mechanisms of interleukin-10-mediated immune suppression. *Immunology* **103**, 131–136 (2001).
48. Brown, M. A. & Hural, J. Functions of IL-4 and control of its expression. *Crit. Rev. Immunol.* **17**, 1–32 (1997).
49. Goswami, R. & Kaplan, M. H. A brief history of IL-9. *J. Immunol.* **186**, 3283 (2011).
50. Harlin, H. et al. Chemokine expression in melanoma metastases associated with CD8<sup>+</sup> T-cell recruitment. *Cancer Res.* **69**, 3077–3085 (2009).
51. Sivick, K. E. et al. Magnitude of therapeutic STING activation determines CD8<sup>+</sup> T cell-mediated anti-tumor immunity. *Cell Rep.* **25**, 3074–3085.e3075 (2018).
52. Lechner, M. G. et al. Immunogenicity of murine solid tumor models as a defining feature of in vivo behavior and response to immunotherapy. *J. Immunother.* **36**, 477–489 (2013).
53. Fitzgerald-Bocarsly, P., Dai, J. & Singh, S. Plasmacytoid dendritic cells and type I IFN: 50 years of convergent history. *Cytokine Growth Factor Rev.* **19**, 3–19 (2008).
54. Liang, H. et al. Host STING-dependent MDSC mobilization drives extrinsic radiation resistance. *Nat. Commun.* **8**, 1736 (2017).
55. Spitzer, M. H. et al. Systemic immunity is required for effective cancer immunotherapy. *Cell* **168**, 487–502.e415 (2017).
56. Poncette, L., Bluhm, J. & Blankenstein, T. The role of CD4 T cells in rejection of solid tumors. *Curr. Opin. Immunol.* **74**, 18–24 (2022).

57. Schadt, L. et al. Cancer-cell-intrinsic cGAS expression mediates tumor immunogenicity. *Cell Rep.* **29**, 1236–1248.e1237 (2019).
58. Carozza, J. A. et al. Extracellular cGAMP is a cancer-cell-produced immunotransmitter involved in radiation-induced anticancer immunity. *Nat. Cancer* **1**, 184–196 (2020).

**Publisher's note** Springer Nature remains neutral with regard to jurisdictional claims in published maps and institutional affiliations.

Springer Nature or its licensor (e.g. a society or other partner) holds exclusive rights to this article under a publishing agreement with the author(s) or other rightsholder(s); author self-archiving of the accepted manuscript version of this article is solely governed by the terms of such publishing agreement and applicable law.

© The Author(s), under exclusive licence to Springer Nature Limited 2023

## Methods

### Materials

All the reagents and solvents were purchased from Sigma-Aldrich, unless otherwise stated. Peptides (H-Cys-Arg-Arg-Arg-NH<sub>2</sub>, H-Cys-Lys-Lys-Lys-NH<sub>2</sub> and H-Cys-His-His-His-NH<sub>2</sub>) were obtained from CPC Scientific with a purity of at least 90%. ML-317 and ML-317-Linker (Supplementary Information) were provided by Takeda Pharmaceuticals.

### Synthesis and characterization of pBAE polymers

Polymers were synthesized in accordance with our previous work, by the addition reaction of primary amines to an excess of diacrylate, resulting in an acrylate-terminated polymer. C6 polymerization was performed by mixing 5-amino-1-pentanol (0.426 g, 4.1 mmol), hexylamine (0.422 g, 4.1 mmol) and 1,4-butanediol diacrylate (2.000 g, 9.1 mmol) under magnetic stirring at 90 °C for 24 h. C32 polymerization was performed by mixing 5-amino-1-pentanol (0.852 g, 8.2 mmol) and 1,4-butanediol diacrylate (2.000 g, 9.1 mmol) under magnetic stirring at 90 °C for 24 h. For the synthesis of cationic pBAE polymers, C6 polymer was end-capped with different thiol-terminated peptides at a 1.0:2.1 molar ratio in dimethyl sulfoxide overnight and collected by precipitation in a mixture of diethyl ether and acetone (7:3 v/v) and dried in vacuo. For the synthesis of CDN or fluorescent polymer, C32 polymer was end-capped with methyl-3-furanthiol at 1.0:2.5 molar ratio in tetrahydrofuran overnight and collected by precipitation in diethyl ether and dried in vacuo. The resultant polymer was end-capped with maleimide-modified CDN or Alexa Fluor 647 C2 Maleimide (Thermo Fisher) at 1:2 molar ratio in dimethyl sulfoxide. The synthesized products were dissolved in an appropriate deuterated solvent and structures were confirmed by <sup>1</sup>H nuclear magnetic resonance (NMR), recorded in a 400 MHz Varian system (NMR Instruments) (Supplementary Figs. 3–9).

### Polymer degradation study

The pBAE degradation rate was measured by diluting free polymer in solution in 100 mM buffers of pH 5.8, 6.8 or 7.4 (final polymer concentration, 0.25 mg ml<sup>-1</sup>). Samples were incubated at 37 °C under shaking. At various time points, samples containing polymer (5 mg) were removed, snap frozen in liquid nitrogen and lyophilised 48 h before being analysed by <sup>1</sup>H NMR.

### Formation of electrostatic and conjugated CDN-NPs

Electrostatic CDN-NPs were generated by mixing equal volumes of CDN at 0.05 mg ml<sup>-1</sup> and pBAE-CR3 polymer at 5.00 mg ml<sup>-1</sup> in sodium acetate buffer at 12.5 mM, followed by 10 min incubation at room temperature. Next, this mixture was nanoprecipitated with two volumes of PBS resulting in the formation of discrete NPs. CDN-conjugated NPs (CDN-NP) were prepared by mixing 25 µl pBAE-CR3 polymer (100 mg ml<sup>-1</sup>), 20 µl pBAE-TCDN-2 (4 mg ml<sup>-1</sup>) and 5 µl of pBAE-AF647 (2 mg ml<sup>-1</sup>) in dimethyl sulfoxide. Then, 450 µl of sodium acetate buffer at 12.5 mM was added to the polymer solution and mixed by pipetting, followed by 10 min incubation at room temperature. For the formation of CDN-NPs, this mixture was nanoprecipitated with 2 ml PBS. Finally, 230 µl of NHS-PEG (2 kDa, Laysan Bio) (10 mg ml<sup>-1</sup>) was added to the NPs and reacted overnight at room temperature. CDN-NP PEGylation was quantified by <sup>1</sup>H-NMR analysis. The final CDN-NPs were purified and concentrated using centrifugal filtration (molecular weight cut-off, 10 kDa) and filtered through a sterile 0.22 µm membrane.

### Biophysical characterization of CDN-NPs

The size and surface charge of NPs were determined by dynamic light scattering using a Zetasizer Nano ZS equipped with a He-Ne laser ( $\lambda = 633$  nm) at a scattering angle of 137° (Malvern Instruments). Electrostatic CDN formulations were further characterized by agarose gel retardation assay. To assess CDN complexation, different ratios of

fluorescent CDN (Ap-8-Fluo-AETGp) to polymer (w:w) between 10:1 and 400:1 were studied. The CDN-polyplexes were freshly prepared and loaded in 4% E-Gel Precast Agarose Gels (Thermo Fisher), run as per the manufacturer's instructions, and visualized in the fluorescence mode.

### Quantification of CDN

The CDN content was determined by LC-MS/MS. CDN-NP-containing samples were incubated with an equal volume of papain digestion solution at 37 °C for 24 h. Next, 40 µl of the previous solution was mixed with 300 µl of 0.1% (v/v) formic acid in methanol containing 150 nM carbutamide (internal standard) for 10 min before LC-MS/MS analysis.

### CDN-NP stability studies

The CDN-NPs were stored in PBS at 4 °C for up to 1 month. The biophysical properties of the resultant CDN-NPs were determined by dynamic light scattering and the functionality of those CDN-NPs was tested in vitro using the RAW reporter cell line. To determine the stability of CDN-NPs in plasma, CDN-NPs were incubated in mouse plasma at 37 °C and free CDN was quantified by LC-MS/MS at different time points as previously described.

### Cell lines

*Mus musculus* skin melanoma (B16-F10 and B16-F10 STING KO, from ATCC), *M. musculus* colon fibroblast (CT-26, from ATCC) and *M. musculus* mammary gland (4T1, from ATCC) were maintained in Dulbecco's minimum essential medium supplemented with 10% (v/v) foetal bovine serum (FBS), 100 U ml<sup>-1</sup> penicillin, 100 µg ml<sup>-1</sup> streptomycin and 2 mM L-glutamine. RAW-Lucia ISG cells and RAW-Lucia ISG STING KO cells (InvivoGen) were similarly maintained with the addition of 100 µg ml<sup>-1</sup> Normocin and Zeocin. Human monocyte THP1-Dual cells and THP1-Dual STING KO cells (InvivoGen) were maintained in RPMI 1640 supplemented with 10% (v/v) FBS, 2 mM L-glutamine, 25 mM HEPES, 100 µg ml<sup>-1</sup> Normocin and 100 µg ml<sup>-1</sup> Zeocin, 10 µg ml<sup>-1</sup> Blastidicin (InvivoGen), 100 U ml<sup>-1</sup> penicillin and 100 µg ml<sup>-1</sup> streptomycin. All the cell lines were maintained in a humidified incubator at 37 °C, 5% CO<sub>2</sub>.

### CDN-NP cell internalization and endocytosis mechanism

To quantify the relative avidity for CDN-NPs, the cells were seeded at  $1 \times 10^5$  cells per well and incubated with fluorescently labelled CDN-NPs at CDN concentrations ranging from 0 to 1,000 nM. After 2 h, excess NPs were removed and the cells were washed, trypsinized and fixed with 4% (v/v) paraformaldehyde for 10 min. The fluorescent NPs were detected using flow cytometry using a 640 nm excitation laser and 670/30 nm filter configuration on a BD LSRFortessa cell analyser. To evaluate the internalization mechanism of CDN-NPs, the cells were treated with several internalization inhibitors. Briefly, the cells were seeded at a density of  $2 \times 10^5$  cells per well in 24-well plates and grown for 24 h before the incubation of inhibitors and CDN-NPs. The cells were then treated with chlorpromazine (28.0 µM), filipin 3 (3.5 µM), rottlerin (10.0 µM), brefeldin A (1.0 µM), chloroquine (10.0 µM) and EIPA (50.0 µM) in the complete culture medium for 60 min at 37 °C. After that, CDN-NPs (100 nM) were added and incubated for 3 h. Subsequently, the cells were analysed by flow cytometry and representative images of the cells were taken with an EVOS M5000 Imaging System microscope. To study the endocytosis mechanism, the cells were seeded in 35 mm glass-bottom dishes (MatTek) at a density of 50,000 cells per dish. After 24 h, the media was switched to OptiMEM with either early or late endosome-GFP trackers for 17 h (Cell Light Early/Late Endosomes-GFP, BACMan 2.0, Thermo Fisher). Then, the cells were incubated with 100 nM CDN-NPs in OptiMEM media for 6 or 24 h and fixed. The samples were preserved with mounting media (ProLong Diamond Antifade Mountant, Thermo Fisher) and imaged by confocal microscopy (EVOS M5000 Imaging System microscope).

### In vitro evaluation of CDN-NPs

Cell viability was assessed using the MTS assay (Promega) as per the manufacturer's instructions. To test CDN-NP activity, human monocyte THP1-Dual cells, THP1-Dual STING KO cells, RAW-Lucia ISG cells and RAW-Lucia ISG STING KO cells were seeded in 96-well plates at  $1 \times 10^5$  cells per well and incubated with the CDN-NP or free CDN at CDN concentrations ranging from 0 to 500 nM. At 24 h post-treatment, IRF3 activity was examined using the QUANTI-Luc reagent (InvivoGen) and the NF- $\kappa$ B activity (only THP1-Dual cells) was determined using the QUANTI-Blue reagent (InvivoGen) according to the manufacturer's instructions.

### Mouse care and experimentation

Female WT C57BL/6 and BALB/c mice (6–8 weeks old) were purchased from Charles River. C57BL/6J-*Sting*<sup>fl/fl</sup> (goldenticket) mice were purchased from the Jackson Laboratory. Animal research and veterinary care were performed at the Hale Building for Translational Medicine, the Koch Institute for Integrative Cancer Research and Takeda Boston under the protocol approved for this study by the Institutional Animal Care and Use Committee.

### BMDC and BMDM isolation

The tibiae and femurs of female WT or goldenticket C57BL/6 mice (aged 8–12 weeks) were isolated and flushed to harvest the bone marrow and to obtain a progenitor cell population<sup>59</sup>. To generate BMDMs,  $4\text{--}6 \times 10^6$  bone marrow cells were cultured in non-tissue culture-treated T175 flasks with 25 ml Dulbecco's minimum essential medium/F12 supplemented with 10% (v/v) FBS, 1% (v/v) penicillin–streptomycin, 5% (v/v) GlutaMAX and recombinant murine macrophage colony-stimulating factor ( $20 \text{ ng ml}^{-1}$ ). The flasks were supplemented with additional medium on days 3 and 6. To generate BMDCs,  $2 \times 10^6$  bone marrow cells were added to non-tissue culture-treated Petri dishes and cultured in 10 ml RPMI 1640 supplemented with 10% (v/v) FBS, 1% (v/v) penicillin–streptomycin and recombinant murine granulocyte macrophage colony-stimulating factor ( $20 \text{ ng ml}^{-1}$ ), 10 ml more of which was added on day 3. On day 6 and every other day thereafter until use, 10 ml of the consumed medium was centrifuged and replaced with 10 ml of fresh medium. To collect the cells, BMDMs were detached using Accumax and BMDCs were loosely adherent and could be collected by simple washing.

### Assessment of primary immune cell activation

BMDCs or BMDMs were seeded in 24-well plates at  $2 \times 10^5$  cells per well and incubated with the CDN-NP or free CDN at equal CDN concentrations ranging from 1 to 100 nM. Empty-NPs were also used at the equivalent polymer concentration. After 24 h, the supernatant was removed and the cells were collected, washed, stained, fixed and analysed by flow cytometry. The following antibodies were used: CD45 BV785 (clone 30-F11), CD11b BV421 (clone M1/70), F4/80 BUV395 (clone T45-2342), MHCII BV605 (clone M5/114.15.2), CD11c BV421 (clone N418), CD86 BB515 (clone GL-1), CD80 APC (clone 16-10A1) and CD206 PE (clone C068C2). Live cells were gated using LIVE/DEAD (Thermo Fisher) near-IR (cat. no. L34976).

### PK of CDN-NPs

Non-tumour-bearing 6–8-week-old female C57BL/6 mice were intravenously injected (100  $\mu$ l per mouse) with fluorescent CDN-NPs and whole blood was collected 0.25, 0.50, 1.00, 3.00, 6.00 and 24.00 h post-injection in Eppendorf tubes containing heparin through submandibular bleed (for early time points) or cardiac puncture (for late time points). Plasma was obtained by centrifugation for 20 min at  $10,000 \times g$ . Fluorescent CDN-NPs were quantified using a 640 nm excitation and 680 emission wavelength by a plate reader, and the CDN was also quantified by LC-MS/MS.

### BD and cellular localization of CDN-NPs

C57BL/6 mice bearing B16-F10 tumours ( $\sim 100 \text{ mm}^3$ ) were intravenously injected with fluorescent CDN-NPs and euthanized at 6, 24 and 48 h after injection. Tumour, tdLN, liver, lungs, heart, kidneys and spleen were collected, imaged using an in vivo imaging system (IVIS), and digested using Precellys lysing kits (Bertin Instruments) following the manufacturer's instructions. Fluorescent CDN-NP distribution was quantified by referencing to a standard curve and the background fluorescence was removed by subtracting the baseline fluorescence values of tissue lysates from PBS-treated mice. CDN was also quantified by LC-MS/MS as described above. To determine the cellular populations that contained CDN-NPs, mice bearing B16-F10 tumours were treated as described above and were euthanized 4 and 24 h post-injection. The tumour, tdLN, spleen and liver were collected; dissociated into single-cell suspensions; and stained, fixed, washed and resuspended in a cell-staining buffer (BioLegend). The following antibodies were used: CD45 APC-Cy7 (clone 30-F11), CD45 BV785 (clone 30-F11), NK-1.1 BV710 (clone PK136), CD3 BB700 (clone 17A2), CD8a BV421 (clone 53-6.7), CD4 BUV395 (clone GK1.5), CD11b BV421 (clone M1/70), F4/80 BUV395 (clone T45-2342), Ly-6C APC-Cy7 (clone HK1.4), Ly-6G BV661 (clone 1A8), MHCII BV605 (clone M5/114.15.2) and CD11c BV421 (clone N418). Live cells were gated using LIVE/DEAD (Thermo Fisher) aqua (cat. no. L34966), green (cat. no. L34970) or near-IR (cat. no. L34976). Cells were analysed by flow cytometry using a BD LSRFortessa flow cytometer (BD Biosciences) and analysed using FlowJo software (v.10.8).

### In vivo therapeutic efficacy

B16-F10, 4T1 and CT-26 cells were subcutaneously injected into the right flank of 6–8-week-old female mice (of the appropriate background for the cell type) in 100  $\mu$ l Hanks' Balanced Salt solution (HBSS) at densities of  $5 \times 10^5$ ,  $1 \times 10^6$  and  $1 \times 10^6$  cells per injection, respectively. Seven days after tumour inoculation ( $\sim 50 \text{ mm}^3$ ), the mice were subjected to intravenous injection (100  $\mu$ l) of free CDN or CDN-NPs at a CDN dose of 0.5  $\mu$ g. Mice were injected three times with treatments spaced four days apart. Groups receiving checkpoint blockade were intraperitoneally injected 24 h after systemic administration with 100  $\mu$ g anti-PD-1 (clone RMP1.14, Bio X Cell). The tumour size was measured every other day via caliper measurements and the tumour volume was calculated using the equation  $V = L \times W \times H \times \frac{\pi}{6}$ . Body weight was contemporaneously measured with the tumour volume. The mice were euthanized when the tumours reached a volume of 1,000  $\text{mm}^3$  or exhibited poor body condition.

### STING-dependent therapeutic efficacy

To confirm the STING-dependent antitumour activity, WT or goldenticket female C57BL/6 mice (6–8 weeks old) were subcutaneously inoculated with either WT B16-F10 tumour cells or STING KO B16-F10 tumour cells. To study STING-dependent therapeutic efficacy in spleen-deficient mice, C57BL/6 mice were splenectomized one week before the therapeutic efficacy studies and B16-F10 tumours were implanted as described above. In both cases, seven days after tumour inoculation ( $\sim 50 \text{ mm}^3$ ), the mice were subjected to an intravenous injection (100  $\mu$ l) of CDN-NPs (0.5  $\mu$ g) with or without anti-PD-1 (100  $\mu$ g) following the same dose regimen described above. Tumour size and survival were monitored until the tumours reached a volume of 1,000  $\text{mm}^3$  or exhibited poor body condition.

### Immunophenotyping analysis

Subcutaneous B16-F10 tumours were established in female C57BL/6 mice (6–8 weeks old), as previously described. The treatment groups were PBS (untreated control), anti-PD-1, free CDN, free CDN with anti-PD-1, CDN-NPs, and CDN-NPs with anti-PD-1. CDN formulations (free drug or NP, 0.5  $\mu$ g CDN) were intravenously administered and anti-PD-1 (100  $\mu$ g) was intraperitoneally administered 24 h after CDN

treatment. DCs and macrophages were assessed 48 h after treatment and T cells were analysed seven days post-treatment. Tumours were harvested, chopped and digested in a solution of HBSS supplemented with collagenase I, II and IV (100 ng ml<sup>-1</sup>) and DNase I (1 µg ml<sup>-1</sup>) for 2 h at 37 °C. The tdLNs and spleens were harvested and mechanically dissociated. Single cell suspensions of tumours, tdLNs and spleens were filtered through a 40 µm nylon cell strainer. Spleen and tumour cells were further treated with ACK Lysing Buffer (Gibco). The cells were washed, filtered through a 40 µm nylon cell strainer and counted. For intracellular IFN $\gamma$  cytokine analysis, 1 × 10<sup>6</sup> cells were seeded in a 24-well plate in Dulbecco's minimum essential medium containing 10% (v/v) FBS and supplemented with PMA/ionomycin/brefeldin A cocktail (BioLegend). After 4 h, the cells were washed and stained in 100 µl cell staining buffer (BioLegend). Intracellular staining was performed using an intracellular staining permeabilization wash buffer (BioLegend). The following anti-mouse antibodies were used for flow cytometry and were purchased from BioLegend: CD45 APC-Cy7 (clone 30-F11), NK-1.1 BV710 (clone PK136), IFN $\gamma$  BV421 (clone XMGL2), CD279 (PD-1) FITC (clone 29.F.1A12), CD45 BV785 (clone 30-F11), CD11b BV421 (clone M1/70), Ly-6C APC-Cy7 (clone HK1.4), Ly-6G BV661 (clone 1A8), CD8a BV421 (clone 53-6.7), CD86 BV510 (clone GL-1), CD80 BV711 (clone 16-10A1), CD206 PE (clone C068C2), MHCII BV605 (clone M5/114.15.2), CD11c APC (clone N418), Siglec H PE (clone 551) and CD44 BV786 (clone IM7). The following anti-mouse antibodies were purchased from BD Biosciences: CD3 BB700 (clone 17A2), CD4 BUV395 (clone GK1.5), CD8a BUV737 (clone 53-6.7), F4/80 BUV395 (clone T45-2342), CD103 BUV395 (clone M290), CD80 BUV737 (clone 16-10A1), ki67 BV510 (clone B56), CD69 BV605 (clone H1.2F3) and CD62L PE-CF594 (clone MEL-14). Live cells were gated using LIVE/DEAD (Thermo Fisher) aqua (cat. no. L34966), green (cat. no. L34970) or near-IR (cat. no. L34976). The stained cells were analysed by flow cytometry using a BD LSRFortessa flow cytometer (BD Biosciences) and all the data were analysed using FlowJo software (FlowJo). Supplementary Figs. 49 and 50 show the gating strategy.

### Cytokine analysis

Female C57BL/6 mice (6–8 weeks old) bearing B16-F10 tumours were given one i.v. injection of PBS, free CDN and CDN-NPs at a dose of 0.5 µg or Empty-NP (non-CDN-containing NPs at an equivalent polymer concentration). After 4 h, the mice were euthanized and the tumours, tdLNs and spleens were harvested and blood was collected, after which plasma was obtained by centrifugation. Tissues were lysed with 0.5% (v/v) CHAPS containing protease and phosphatase inhibitors. Levels of IFN $\gamma$ , IFN- $\beta$ , IFN- $\alpha$  (MSD U-Plex interferon combo, cat. no. K15320K-2), IL-1 $\beta$ , IL-2, IL-4, IL-5, IL-6, IL-9, KC/GRO, IL-10, IL-12p70 (MSD Proinflammatory Panel, cat. no. K15045G-2), tumour necrosis factor, IL-15, IL-17A/F, IL-27p28/IL-30, L-33, IP-10, MCP-1, MIP-1 $\alpha$  and MIP-2 (MSD Cytokine Panel, cat. no. K15245D-2) were measured according to the manufacturer's instructions.

### Cellular transfer of CDN-NPs

Wild-type and STING KO B16-F10 cells in a T-75 tissue culture flask at a confluency of 80–90% were treated for 4 h with free CDN, Empty-NPs or CDN-NPs at equivalent doses. The cells were then washed, trypsinized and seeded in 24-well plates at a density of 1 × 10<sup>5</sup> cells per well. Once the cells were attached, 1 × 10<sup>5</sup> immune cells (WT and STING KO THP1-Dual, RAW-Lucia ISG, BMDC and BMDM) were added to the wells and incubated for 24 h. In the case of the immortalized reporter cell lines, the supernatant was analysed according to the manufacturer's instructions. For experiments involving primary immune cells, the cells were collected, washed, stained, fixed and analysed by flow cytometry. For in vivo studies, B16-DsRed, B16-F10 or B16-F10 STING KO cells were identically treated, as above, via subcutaneous implantation in the right flank of female C57BL/6 mice (5 × 10<sup>5</sup> cells per injection in 100 µl HBSS). Cells treated with Empty-NPs alone at an equivalent

polymer concentration were used as the control. For efficacy studies, the tumours were monitored until the humane endpoint was reached. For mechanistic studies, tumours and tdLN were isolated at one, two and seven days post-tumour inoculation. The DCs and macrophages were isolated by flow cytometry and the percentage of fluorescent CDN-NPs and B16-DsRed cancer cells was determined.

### Haematoxylin and eosin staining

B16-F10 tumour-bearing C56BL/6 mice were systemically injected with CDN-NPs containing 0.5 µg CDN. At two and seven days post-administration, the spleens and livers were collected, kept in 10% (v/v) formalin for a minimum of 24 h and then in 70% (v/v) ethanol until processing. Haematoxylin and eosin was assessed from histological sections (5 µm) following standard protocols.

### Statistical analysis

Statistical analyses were carried out using Prism 9 software (GraphPad). All the data are reported as mean ± standard error of the mean (s.e.m.). For in vitro experiments, a minimum of  $n = 3$  biological replicates were used per condition in each experiment. Pair-wise comparisons were performed using Student's  $t$ -tests. Multiple comparisons among groups were determined using one-way analysis of variance (ANOVA) or two-way ANOVA with Bonferroni's multiple-comparisons tests. For in vivo experiments, a minimum of  $n = 5$  biological replicates were used per condition in each experiment. Kaplan–Meier survival curves statistical analysis was determined using a two-tailed Mantel–Cox test.

### Reporting summary

Further information on research design is available in the Nature Portfolio Reporting Summary linked to this article.

### Data availability

All data generated or analysed that support the findings of this study are available within this Article and its Supplementary Information. All raw data from this study are available from the corresponding author upon request. Source data are provided with this paper.

### References

59. Madaan, A., Verma, R., Singh, A. T., Jain, S. K. & Jaggi, M. A stepwise procedure for isolation of murine bone marrow and generation of dendritic cells. *J. Biol. Methods* **1**, e1 (2014).

### Acknowledgements

We are grateful for the support and funding of Takeda Pharmaceuticals. We thank the Hale Building for Transformative Medicine, the Koch Institute for Integrative Cancer Research at the Massachusetts Institute of Technology (MIT) and at Takeda Boston for the assistance with animal housing. We also thank A. M. Hayward and P. Chamberlain from the Department of Comparative Medicine at MIT for animal assistance, G. Paradis for FACS assistance with Cancer Center Support (FACS core) and K. Cormier for histology assistance.

### Author contributions

P.D., A.O.A.-Y. and N.A. conceived the study. P.D. designed the experiments. S.P.L., D.L., J.W. and S.H. performed the ML-317 synthesis and quantification. P.D., A.M.C., M.Z.D., D.L., J.W., S.H., G.M.T., N.P., S.F., M.P. and A.L.R. performed the in vitro experiments. P.D., A.M.C., S.K., T.H., M.L.G. and V.A.A. performed the in vivo experiments. P.D., A.M.C., M.Z.D. and N.A. drafted and finalized the manuscript with input from all other authors.

### Competing interests

The authors declare no competing interests.



**Additional information**

**Supplementary information** The online version contains supplementary material available at <https://doi.org/10.1038/s41565-023-01447-7>.

**Correspondence and requests for materials** should be addressed to Pere Dosta or Natalie Artzi.

**Peer review information** *Nature Nanotechnology* thanks Jordan Green, Jason Luke and the other, anonymous, reviewer(s) for their contribution to the peer review of this work.

**Reprints and permissions information** is available at [www.nature.com/reprints](http://www.nature.com/reprints).

## Reporting Summary

Nature Portfolio wishes to improve the reproducibility of the work that we publish. This form provides structure for consistency and transparency in reporting. For further information on Nature Portfolio policies, see our [Editorial Policies](#) and the [Editorial Policy Checklist](#).

### Statistics

For all statistical analyses, confirm that the following items are present in the figure legend, table legend, main text, or Methods section.

- | n/a                                 | Confirmed  |
|-------------------------------------|--|
| <input type="checkbox"/>            | <input checked="" type="checkbox"/> The exact sample size ( $n$ ) for each experimental group/condition, given as a discrete number and unit of measurement  |
| <input type="checkbox"/>            | <input checked="" type="checkbox"/> A statement on whether measurements were taken from distinct samples or whether the same sample was measured repeatedly  |
| <input type="checkbox"/>            | <input checked="" type="checkbox"/> The statistical test(s) used AND whether they are one- or two-sided<br><i>Only common tests should be described solely by name; describe more complex techniques in the Methods section.</i>   |
| <input checked="" type="checkbox"/> | <input type="checkbox"/> A description of all covariates tested  |
| <input type="checkbox"/>            | <input checked="" type="checkbox"/> A description of any assumptions or corrections, such as tests of normality and adjustment for multiple comparisons  |
| <input type="checkbox"/>            | <input checked="" type="checkbox"/> A full description of the statistical parameters including central tendency (e.g. means) or other basic estimates (e.g. regression coefficient) AND variation (e.g. standard deviation) or associated estimates of uncertainty (e.g. confidence intervals) |
| <input type="checkbox"/>            | <input checked="" type="checkbox"/> For null hypothesis testing, the test statistic (e.g. $F$ , $t$ , $r$ ) with confidence intervals, effect sizes, degrees of freedom and $P$ value noted<br><i>Give <math>P</math> values as exact values whenever suitable.</i>                            |
| <input checked="" type="checkbox"/> | <input type="checkbox"/> For Bayesian analysis, information on the choice of priors and Markov chain Monte Carlo settings  |
| <input checked="" type="checkbox"/> | <input type="checkbox"/> For hierarchical and complex designs, identification of the appropriate level for tests and full reporting of outcomes  |
| <input checked="" type="checkbox"/> | <input type="checkbox"/> Estimates of effect sizes (e.g. Cohen's $d$ , Pearson's $r$ ), indicating how they were calculated  |

*Our web collection on [statistics for biologists](#) contains articles on many of the points above.*

### Software and code

Policy information about [availability of computer code](#)

**Data collection** DLS analysis was collected using a Zetasizer ZS with Zetasizer software (v. 7.13). Flow cytometric data were collected using BD FACSDiva software (v. 9.0). In vivo images were acquired using IVIS spectrum with Living Image software (v.4.7.4). Luminescence and fluorescence data were collected using multimodal plate reader (infinite M plex, TECAN) using inbuilt software (v. 5.26).

**Data analysis** DLS analysis was done in Zetasizer software (v. 7.13). Flow cytometry analysis was performed in FlowJo (v.10.8). In vivo images were analyzed using IVIS Spectrum Living Image Software (v. Statistical analysis was performed using GraphPad Prism 9.0.

For manuscripts utilizing custom algorithms or software that are central to the research but not yet described in published literature, software must be made available to editors and reviewers. We strongly encourage code deposition in a community repository (e.g. GitHub). See the Nature Portfolio [guidelines for submitting code & software](#) for further information.

### Data

Policy information about [availability of data](#)

All manuscripts must include a [data availability statement](#). This statement should provide the following information, where applicable:

- Accession codes, unique identifiers, or web links for publicly available datasets
- A description of any restrictions on data availability
- For clinical datasets or third party data, please ensure that the statement adheres to our [policy](#)

The authors declare that data supporting the findings of this study are available within the article and its Supplementary Information files. All relevant data can be provided by the authors upon reasonable request. The raw and analysed datasets generated during the study are too large to be publicly distributed, but they are available for research purposes from the corresponding author on reasonable request.

## Field-specific reporting

Please select the one below that is the best fit for your research. If you are not sure, read the appropriate sections before making your selection.

- Life sciences       Behavioural & social sciences       Ecological, evolutionary & environmental sciences

For a reference copy of the document with all sections, see [nature.com/documents/nr-reporting-summary-flat.pdf](https://www.nature.com/documents/nr-reporting-summary-flat.pdf)

## Life sciences study design

All studies must disclose on these points even when the disclosure is negative.

Sample size	Sample sizes were based on previous experimental data generated in-house as well as in previous publications ( <a href="https://www.nature.com/articles/s41565-018-0342-5">https://www.nature.com/articles/s41565-018-0342-5</a> , <a href="https://www.nature.com/articles/s41565-021-00962-9">https://www.nature.com/articles/s41565-021-00962-9</a> ),
Data exclusions	No data was excluded
Replication	All experiments were repeated at least twice, without significant differences in their outcome
Randomization	In all experiments, with or without mice, groups were randomly assigned.
Blinding	Investigators were blinded during to group allocation during data collection and analysis.

## Reporting for specific materials, systems and methods

We require information from authors about some types of materials, experimental systems and methods used in many studies. Here, indicate whether each material, system or method listed is relevant to your study. If you are not sure if a list item applies to your research, read the appropriate section before selecting a response.

### Materials & experimental systems

- |                                     |   |
|-------------------------------------|---|
| n/a                                 | Involved in the study   |
| <input type="checkbox"/>            | <input checked="" type="checkbox"/> Antibodies                  |
| <input type="checkbox"/>            | <input checked="" type="checkbox"/> Eukaryotic cell lines       |
| <input checked="" type="checkbox"/> | <input type="checkbox"/> Palaeontology and archaeology          |
| <input type="checkbox"/>            | <input checked="" type="checkbox"/> Animals and other organisms |
| <input checked="" type="checkbox"/> | <input type="checkbox"/> Human research participants            |
| <input checked="" type="checkbox"/> | <input type="checkbox"/> Clinical data                          |
| <input checked="" type="checkbox"/> | <input type="checkbox"/> Dual use research of concern           |

### Methods

- |                                     |  |
|-------------------------------------|--|
| n/a                                 | Involved in the study                              |
| <input checked="" type="checkbox"/> | <input type="checkbox"/> ChIP-seq                  |
| <input type="checkbox"/>            | <input checked="" type="checkbox"/> Flow cytometry |
| <input checked="" type="checkbox"/> | <input type="checkbox"/> MRI-based neuroimaging    |

## Antibodies

### Antibodies used

Rat anti-mouse PD-1 (clone RMO1-14, BioXCell) (dilution depended on concentration of stock from manufacturer, 100ug/mouse)  
 APC/Cy7-conjugated rat anti-mouse CD45 (clone 30-F11, Biolegend, 1:100)  
 BV711-conjugated mouse anti-mouse NK-1.1 (clone PK136, Biolegend, 1:100)  
 BV421-conjugated rat anti-mouse IFN-γ (clone XMG1.2, BD Biosciences, 1:100)  
 FITC-conjugated rat anti-mouse CD279 (PD-1) (clone 29F.1A12, Biolegend, 1:100)  
 BV785-conjugated rat anti-mouse CD45 (clone 30-F11, Biolegend, 1:100)  
 BV421-conjugated rat anti-mouse CD11b (clone M1/70, Biolegend, 1:50)  
 APC/Cy7-conjugated rat anti-mouse Ly-6C (clone HK1.4, Biolegend, 1:200)  
 BV661-conjugated rat anti-mouse Ly-6G (clone 1A8, Biolegend, 1:200)  
 BV421-conjugated rat anti-mouse CD8a (clone 53-6.7, Biolegend, 1:400)  
 BV510-conjugated rat anti-mouse CD86 (clone GL-1, Biolegend 1:200)  
 BV711-conjugated hamster anti-mouse CD80 (clone 16-10A1, Biolegend, 1:200)  
 PE-conjugated rat anti-mouse CD206 (clone C068C2, Biolegend, 1:200)  
 BV605-conjugated rat anti-mouse MHCII (clone M5/114.15.2, Biolegend, 1:200)  
 APC-conjugated hamster anti-mouse CD11c (clone N418, Biolegend, 1:200)  
 PE-conjugated rat anti-mouse Siglec H (clone 551, Biolegend, 1:100)  
 BV786-conjugated rat anti-mouse CD44 (clone IM7, Biolegend, 1:100)  
 BB700-conjugated rat anti-mouse CD3 (clone 17A2, BD Biosciences, 1:100)  
 BUV395-conjugated rat anti-mouse CD4 (clone GK1.5, BD Biosciences, 1:100)  
 BUV737-conjugated rat anti-mouse CD8a (clone 53-6.7, BD Biosciences, 1:100)  
 BUV395-conjugated rat anti-mouse F4/80 (clone T45-2342, BD Biosciences, 1:200)  
 BUV395-conjugated rat anti-mouse CD103 (clone M290, BD Biosciences, 1:100)  
 BUV737-conjugated hamster anti-mouse CD80 (clone 16-10A1, BD Biosciences, 1:200)  
 BV510-conjugated mouse anti-mouse ki67 (clone B56, BD Biosciences, 1:100)

BV605-conjugated hamster anti-mouse CD69 (clone H1.2F3, Biolegend, 1:100)  
PE-CF594-conjugated rat anti-mouse CD62L (clone MEL-14, BD Biosciences, 1:100)

Validation

All antibody were validated for each specific assay. Antibody validation was provided by manufacture's website (cell images or flow cytometry plots) and/or data provided in the manuscript.

## Eukaryotic cell lines

Policy information about [cell lines](#)

Cell line source(s)

B16-F10, 4T1, and CT26 cell lines were obtained from ATCC. THP1-Dual, THP1-Dual KO-STING, RAW-Lucia ISG, and RAW- cell lines were obtained from Invivogen. B16-F10 KO-STING cell line was obtained from Takeda Pharmaceuticals. B16-DSred cell line was obtained from Koch Institute for Integrative Cancer Research.

Authentication

B16-F10, 4T1, and CT26 cell lines were authenticated by ATCC. THP1-Dual, THP1-Dual KO-STING, RAW-Lucia ISG, and RAW- cell lines were authenticated by Invivogen. B16-F10 KO-STING cell line was authenticated by Takeda Pharmaceuticals. B16-DSred cell line was authenticated by Koch Institute for Integrative Cancer Research. All cell lines were authenticated by STR profiling

Mycoplasma contamination

All cell lines were tested negative for mycoplasma contamination.

Commonly misidentified lines  
(See [ICLAC](#) register)

No commonly misidentified cell lines were used.

## Animals and other organisms

Policy information about [studies involving animals](#); [ARRIVE guidelines](#) recommended for reporting animal research

Laboratory animals

6-8-week-old female BALB/c mice (Charles River, 18 g-20 g)  
6-8- week-old female C57-BL/6 mice (Charles River or Jackson Laboratory, 18 g-20 g)  
6-8- week-old female C57-BL/6 SpleenX mice (Charles River, 18 g-20 g)  
6-8- week-old female C57BL/6J-Sting1gt/J mice (Jackson Laboratory, 18 g-20 g)  
12-week-old female BALB/c mice (Charles River, 18 g-20 g) used for rechallenge studies  
12- week-old female C57-BL/6 SpleenX mice (Charles River, 18 g-20 g) used for rechallenge studies  
Mice were housed in 12h light/12h dark cycle with the temperature maintained between 65-75°F (~18-23°C), ~50% humidity.

Wild animals

No wild animals were used.

Field-collected samples

No field-collected samples were used.

Ethics oversight

Animal research and veterinary care was performed at the Hale Building for Transformative Medicine, the Koch Institute for Integrative Cancer Research at Massachusetts Institute of Technology (MIT), and at Takeda Pharmaceuticals under the protocol approved for this study by the Institutional Animal Care and Use Committee (IACUC).

Note that full information on the approval of the study protocol must also be provided in the manuscript.

## Flow Cytometry

Plots

Confirm that:

- The axis labels state the marker and fluorochrome used (e.g. CD4-FITC).
- The axis scales are clearly visible. Include numbers along axes only for bottom left plot of group (a 'group' is an analysis of identical markers).
- All plots are contour plots with outliers or pseudocolor plots.
- A numerical value for number of cells or percentage (with statistics) is provided.

Methodology

Sample preparation

The sample preparation was described in the Materials and Methods section. Briefly, mouse tissues were enzymatically digested or mechanically processed and serially filtered to obtained a single cell suspension. Samples were then counted and the appropriate downstream staining protocol was followed depending on extracellular or intracellular staining. Cell culture samples were processed similarly except using trypsin or non-enzymatic methods of detachment. Single cell suspensions only were used in all experiments.

Instrument

LSRFortessa HTS-2 and FACS Symphony A3

Software

BD FACSDiva (v. 9.0) was used for the collection. FlowJo (v. 10.8) was used for analysis.

Cell population abundance

From in vitro, cells were collected to obtain at least 10000 events.  
From the in vivo, cells were collected to obtain at least 1000 events in the smallest subpopulation.

Gating strategy

Cells were gated first with SSC-A vs. FSC-A plots. To exclude doublets cells were gated by FSC-H vs. FSC-W and SSC-H vs. SSC-W. Live cells were gated using LIVE/DEAD (Thermo Fisher) aqua (cat. no. L34966), green (cat. no. L34970) or near-IR (cat. no. L34976) stainings

Tick this box to confirm that a figure exemplifying the gating strategy is provided in the Supplementary Information.